FINITE ELEMENT FORMULATIONS OF TIME VARYING MAGNETIC FIELD PROBLEMS

Z.J. Csendes
Corporate Research and Development, General Electric
Schenectady, New York

ABSTRACT

This paper consists of three parts: First, it examines the finite element formulations of time-varying magnetic field problems presently appearing in the literature and shows that all of the existing formulations are derived by using a similar representation of the electromagnetic field. Second, it discusses the nature of finite element discretization and demonstrates the utility of using elementary matrix operators in this process. Third, it derives a new finite element formulation of time-varying magnetic field problems in which the magnetic field is determined directly, without recourse to magnetic potential functions. The treatment is based on a two component vector formulation of magnetic field problems in which the non-divergence of the magnetic field is imposed by using a numerical procedure.

1. INTRODUCTION

The finite element method as applied to electromagnetic field problems is now nearly ten years old, and a number of different field problems have been solved successfully by this technique. The first application of the finite element method to magnetic field problems was the work of Silvester and Chari[1], which treated the two-dimensional nonlinear magnetostatic field problem encountered in electric machine design. Shortly thereafter, the finite element method was extended to the solution of time varying magnetic field problems, again originating with papers by Silvester[2] and by Chari[3], both of which treated eddy-current effects. In these solutions, the magnetic field is assumed to be a linear function of the magnetic flux density and is treated as a complex valued function which is harmonic in time. This procedure has been adapted to different problems by a number of authors who have reported several extensions of the technique[4-8].

A second category of time-varying electromagnetic field problems solved by the finite element method are skin-effect problems in which a net current flows in the conducting region. Solutions of the skin-effect problem have been reported by Chari[9] and Csendes[9] and by Konrad, Coulomb, Sabonnadiere and Silvester[10].

A third category of time-varying magnetic field problem solved by the finite element method is the transient field problem. In this case, the time-varying field is solved as a succession of magnetostatic field problems each at a different point in time, integrating the magnetic field through time to obtain a complete solution. Electromagnetic field problems in this category are solved in References 11-14.

Finally, there is yet another category of time-varying electromagnetic field problems which has been solved by the finite element method. These are field problems involving three-dimensional effects which must be solved using a vector formulation instead of the scalar formulation used elsewhere. The principal papers in the literature in this category are the ones by Okuda[15] and by Becker, Pillsbury and Driga[16].

The purpose of this paper is two-fold: First, it is an attempt to present a unified view of the finite element method as it is applied to the diverse problems mentioned above. The general formulation presented here is made possible by introducing the concept of "elementary matrix operators" to represent the field equations. The second purpose of this paper is to introduce a new formulation of time-varying magnetic field problems in which the magnetic field is solved as a non-divergent vector field quantity. This formulation differs from those appearing in the literature in that the magnetic field is determined directly and not as the curl of the magnetic vector potential.

2. THE ELECTROMAGNETIC FIELD EQUATIONS

The usual starting point for electromagnetic field analysis is Maxwell's equations. In electric machine problems, where displacement currents and charges are negligible, these equations are

$$\begin{aligned} \nabla \times \bar{E} &= -\frac{\partial \bar{B}}{\partial t} \\ \nabla \times \bar{H} &= \bar{J} \\ \nabla \cdot \bar{B} &= 0 \\ \nabla \cdot \bar{D} &= 0 \end{aligned} \qquad (1)$$

The purpose of the following is to derive a general field equation governing all electromagnetic phenomena in electric machines, including those which involve moving media. For this purpose, consider a material of relative permeability, μ_r, relative permittivity ε_r, and conductivity, σ, moving with a velocity $\bar{v}_c$ with respect to an inertial reference frame. According to the principle of space-time covariance, the form of any physical law is unaltered by the relative motion of the observer. Hence, in the moving coordinate system, Maxwell's equations remain unchanged

$$\begin{aligned} \nabla' \times \bar{E}' &= -\frac{\partial \bar{B}'}{\partial t'} \\ \nabla' \times \bar{H}' &= \bar{J}' \\ \nabla \cdot \bar{B}' &= 0 \\ \nabla \cdot \bar{D}' &= 0 \end{aligned} \qquad (2)$$

except that primes are used in Equation 2 to indicate that all quantities are evaluated in the moving coordinate system. It can be shown[17] that under a Galilean space-time transformation, Equation 1 yields

$$\begin{aligned} \nabla' \times (\overline{E} + \overline{V}_c \times \overline{B}) &= -\frac{\partial \overline{B}}{\partial t'} \\ \nabla' \times \overline{H} &= \overline{J} \\ \nabla' \cdot \overline{B} &= 0 \\ \nabla' \cdot \overline{D} &= 0 \end{aligned} \tag{3}$$

Since Equation 3 must be the same as Equation 2, there results

$$\begin{aligned} \overline{E}' &= \overline{E} + \overline{V}_c \times \overline{B} \\ \overline{H}' &= \overline{H} \\ \overline{B}' &= \overline{B} \\ \overline{D}' &= \overline{D} \\ \overline{J}' &= \overline{J} \end{aligned} \tag{4}$$

Thus, in the absence of displacement currents, the electromagnetic field vectors $\overline{H}$, $\overline{B}$, $\overline{D}$ and $\overline{J}$ are unaltered when viewed from a moving coordinate system, but the electric field vector $\overline{E}$ is modified by the addition of the term $\overline{V}_c \times \overline{B}$.

According to the latest experimental evidence[17], the constitutive relationships between electromagnetic field quantities are

$$\begin{aligned} \overline{B} - \mu_o \varepsilon_o \overline{V}_m \times \overline{E} &= \mu_r \mu_o \overline{H} - \mu_r \mu_o \overline{V}_m \times \overline{D} \\ \overline{D} + \mu_o \varepsilon_o \overline{V}_m \times \overline{H} &= \varepsilon_r \varepsilon_o \overline{E} + \varepsilon_r \varepsilon_o \overline{V}_m \times \overline{B} \\ \overline{J} &= \sigma E + \sigma \overline{V}_m \times \overline{B} \end{aligned} \tag{5}$$

where $\overline{V}_m$ is the velocity of the material with respect to an inertial reference frame. Combining Equation 4 and 5 gives

$$\begin{aligned} \overline{D}' &= \varepsilon_r \varepsilon_o \overline{E}' - \mu_o \varepsilon_o (\mu_r \varepsilon_\theta (\overline{V}_m - \overline{V}_c) - \overline{V}_m) \times \overline{H}' \\ \overline{J}' &= \sigma \overline{E}' + \sigma (\overline{V}_m - \overline{V}_c) \times \overline{B}' \end{aligned} \tag{6}$$

Combining Equation 6 with the second Maxwell equation and assuming small velocities yields

$$\nabla' \times \overline{B}' - \sigma \mu_r \mu_o (\overline{V}_m - \overline{V}_c) \times \overline{B}' = \sigma \mu_r \mu_o \overline{E}' \tag{7}$$

Since the divergence of $\overline{B}'$ is zero, the vector $\overline{B}'$ is non-divergent and hence, must be given by the curl of some vector $\overline{A}'$

$$\overline{B}' = \nabla' \times \overline{A}' \tag{8}$$

Substituting Equation 8 into Equation 2 yields

$$\nabla' \times \overline{E}' = -\nabla' \times \frac{\partial \overline{A}'}{\partial t'} \tag{9}$$

Therefore

$$\overline{E}' = -\frac{\partial \overline{A}'}{\partial t} + \nabla \phi \tag{10}$$

Finally, combining Equations 7, 8, and 10 yields

$$\begin{aligned} \nabla'^2 \overline{A}' - \nabla(\nabla \cdot \overline{A}') + \sigma \mu_r \mu_o (\overline{V}_m - \overline{V}_r) \times \nabla \times \overline{A}' \\ - \sigma \mu_r \mu_o \frac{\partial \overline{A}'}{\partial t'} = \sigma \mu_o \mu_r \nabla \phi \end{aligned} \tag{11}$$

Similarly, substituting Equation 10 into the equation $\nabla \cdot \overline{D}' = 0$ implies that

$$\nabla^2 \phi = \frac{\partial}{\partial t} \nabla \cdot \overline{A}' \tag{12}$$

Equations 11 and 12 provide the governing equations for the electromagnetic vector and scalar potentials in electric machines. These equations are solved in References 15 and 16 for some special cases.

3. TWO DIMENSIONAL PROBLEMS

Equations 11 and 12 are simplified considerably in two-dimensional problems where the vector potential $\bar{A}$ has only one component (A_z in Cartesian coordinates, A_θ, in cylinderical coordinates) and is invariant in that component in that direction. Under these conditions, the divergence of the vector potential is automatically zero and Equation 11 becomes

$$\nabla'^2\bar{A}' + \sigma\mu_r\mu_o(\bar{V}_m - \bar{V}_c) \times \nabla \times \bar{A}' - \sigma\mu_r\mu_o \frac{\partial\bar{A}'}{\partial t'} = \mu_r\mu_o \bar{J}_s \qquad (13)$$

where $\bar{J}_s = -\sigma \nabla \phi$ represents external source currents.

Five different cases of Equation 13 are of interest:

I. Magnetostatic Problems. If no conductors are located in the problem region, or if the electromagnetic field problem is invariant in time, Equation 13 reduces to the Poisson equation

$$\nabla^2\bar{A} = -\mu_r\mu_o \bar{J}_s \qquad (14)$$

With reference to the finite element method, this equation was solved by Silvester and Chari[1].

II. Eddy-Current Problems. In the absence of source currents and moving boundaries, and assuming that time variations are sinusoidal, Equation 13 becomes the diffusion equation

$$\nabla^2\bar{A} - j\omega\sigma\mu_r\mu_o \bar{A} = 0 \qquad (15)$$

Equation 15 is solved in References 2-8.

III. Skin-Effect Problems. Skin-effect problems are similar to eddy-current problems, except that external source currents exist. The governing equation is this case is

$$\nabla^2\bar{A} - j\omega\sigma\mu_r\mu_o \bar{A} = -\mu_r\mu_o \bar{J}_s \qquad (16)$$

The skin-effect equation is solved using the finite element method in References 9 and 10.

IV. Moving-Body Problems. In moving boundary problems, adopting a coordinate system moving in unison with the material ($\bar{V}_m = \bar{V}_c$) results in the equation

$$\nabla'^2\bar{A} - j\omega\sigma\mu_r\mu_o \bar{A}' = -\mu_r\mu_o \bar{J}_s \qquad (17)$$

This equation is solved using the finite element method in Reference 8. Another possibility, useful in the linear motor case, is to take a moving coordinate system $\bar{V}_c = \bar{V}$ with a stationary material velocity $\bar{V}_m = 0$. In this case, Equation 13 yields

$$\nabla'^2 A' + \sigma\mu_r\mu_o \bar{V} \times \nabla' \times \bar{A}' - \sigma\mu_r\mu_o \frac{\partial\bar{A}'}{\partial t'} = 0 \qquad (18)$$

Equation 18 is solved in Reference 11.

V. Transient Field Problems. In a transient field problem with no external source currents and with $\bar{V}_m = \bar{V}_c$ Equation 13 reduces to

$$\nabla'^2\bar{A}' - \sigma\mu_r\mu_o \frac{\partial\bar{A}'}{\partial t'} = 0 \qquad (19)$$

The finite element solution of Equation 18 is reported in References 12 through 14.

4. THE FINITE ELEMENT METHOD

Although the finite element method has been applied successfully to a wide variety of problems, its theoretical basis is at times, still misrepresented in the magnetic fields literature. The following analysis is presented to clarify the advantage of using the finite element method to solve magnetic field problems. This analysis is not new; its essential features were originally published by Babuska, Prager, and Vitasek[18].

To begin, let us define a point-valued matrix method (PVMM) to be any procedure for generating approximate solutions of field problems in which point values of the field are determined by solving a matrix equation. Thus, if the governing equation of a field problem is

$$A\ u(x,y) = f(x,y) \qquad (20)$$

then any matrix equation of the form

$$A\ \underset{\sim}{u} = \underset{\sim}{F} \qquad (21)$$

where the components of the column vector $\underset{\sim}{u}$ represent point values of the function $u(x,y)$ provides a PVMM for Equation 20. According to this definition, PVMMs are a very general category of numerical methods for the solution of field problems; both finite difference methods and finite element methods are subcategories of PVMMs.

Although definitions of the finite element method vary in the literature, the most accurate definition of the finite element method is the following: a finite element method is a PVMM in which the matrix A in Equation 21 is determined by using the Galerkin procedure, taking the interpolation functions corresponding to the point values $\underset{\sim}{u}$ to be the basis functions in the Galerkin method. The finite element method is therefore a consistent PVMM in which a specific procedure must be followed to evaluate the elements of the coefficient matrix A.

Of course, any numerical PVMM will have some error: $e_i = u_i - u(x_i,y_i)$ at each point (x_i,y_i) of the solution. A PVMM is called asymtotically optimal if the solution vector $\underset{\sim}{u}$ minimizes the Euclidian norm of the error vector $\underset{\sim}{e}$. The power of the finite element method is a result of the following theorem, first proved in Reference 18: A PVMM will be asymtotically optimal if the elements of the coefficient matrix A of Equation 21 are evaluated by using the Galerkin procedure. Another way of stating this theorem is as follows: All finite element methods are asymtotically optimal.

An immediate consequence of the above theorem is the fact that no finite difference method can be more accurate in the sense of the Euclidian error norm of the point values of the solution than the corresponding finite element method. It is possible, of course, to find solutions of equal accuracy by using the two procedures but, in general, there is no guarantee that the finite difference method will yield asymtotically optimal results. It is for this reason that the finite element method has become so popular in recent years.

5. DISCRETIZATION METHODS

In its simplest form, the procedure for discretizing differential equations by Galerkin's method is as follows: first, one approximates the solution of a field problem by a sum of basis functions $\alpha_i(x,y)$

$$u(x,y) = \sum_{i=1}^{N} u_i \alpha_i(x,y) \tag{22}$$

For notational convenience, it is best to rewrite Equation 22 in the form

$$u(x,y) = \tilde{\alpha}(x,y)\ \underset{\sim}{u} \tag{23}$$

where $\tilde{\alpha}(x,y)$ is the row vector

$$\tilde{\alpha}(x,y) = [\alpha_1(x,y)\ \alpha_2(x,y)\ \ldots\ \alpha_n(x,y)] \tag{24}$$

and $\underset{\sim}{u}$ denotes the column vector

$$\underset{\sim}{u} = \begin{bmatrix} u_1 \\ u_2 \\ \cdot \\ \cdot \\ \cdot \\ u_n \end{bmatrix} \tag{25}$$

The second step in the Galerkin process is to insert the approximation (23) into the operator equation (20). Third, the result is multiplied on the left by the basis functions $\tilde{\alpha}(x,y)$ and integrated over the region of interest. The result is Equation 21, with the coefficient matrix A given by

$$A = \int \tilde{\alpha}^T(x,y)\ \tilde{A}\tilde{\alpha}\ (x,y)\ dxdy$$

where $\tilde{\alpha}^T(x,y)$ denotes the transpose of $\tilde{\alpha}(x,y)$.

Traditionally, the finite element analyst has had two choices for evaluating the integrals in Equation 26. One possibility has been to evaluate the integrals in Equation 26 completely numerically, using numerical quadrature to obtain the required values. This choice has been advocated by Zienkiewicz, among many others, and is today widely used by the civil engineering community. The other possibility has been to evaluate the integrals in Equation 26 analytically using a symbolic manipulation computer language such as Formac, Altran, or Macsyma. This choice was pioneered by Silvester and is used today primarily by electrical engineers.

Both methods of evaluating the Galerkin integrals have advantages and disadvantages. The advantage of the numerical integration procedure is its simplicity and ease of implementation; its disadvantage is high computational cost and, in some cases, lower solution accuracy. The advantages of the analytical integration approach are the high efficiency and high accuracy obtained by using pre-computed matrix elements; its disadvantage is the difficulty of evaluating the many integrals required.

In recent years, however, a third method of evaluating the Galarkin equation matrix elements, called the "elementary matrix approach", has been developed[19-21]. In the elementary matrix approach, differential equations are subdivided into basic units called "elementary operators". Matrix equivalents are evaluated analytically in terms of parametric factors for a representative element for each elementary operator; the

Galerkin matrix for the entire differential equation is obtained by combining the elementary matrix factors numerically.

Three types of elementary matrix operators have been defined: (1) differentiation matrices, (2) function space metric matrices, and (3) projection matrices. All three of these matrices are defined with respect to the basis functions $\tilde{\alpha}(x,y)$, which in finite element analysis are taken to be Nth order interpolation polynomials.

Differentiation Matrices

Differentiation matrices are defined by the equation

$$G_{ij}^{(m)} = \frac{\partial\, \alpha_j^{(N)}(x,y)}{\partial\, \zeta_m} \Bigg|_{x,y = \text{point } i} \tag{26}$$

where $\alpha^{(N)}(x,y)$ is an Nth order interpolation polynomial in the element, ζ_m are homogeneous coordinates in the element, and the symbol $\Big|_{x,y = \text{point } i}$ means that the derivative is to be evaluated at the (N-1)st order interpolation node i.

Function Space Metric Matrices

The function space metric matrix is defined by the equation

$$T = \frac{1}{A}\int \tilde{\alpha}^{(N)^T}(x,y)\, \tilde{\alpha}^{(N)}(x,y)\, dx\, dy \tag{27}$$

where A is the area of the element

Projection Matrices

Projection matrices are defined by the equation

$$P = T^{-1} A \tag{28}$$

where T is the (N-1)st order metric matrix and

$$A = \frac{1}{A}\int \tilde{\alpha}^{(N-1)^T}(x,y)\, \tilde{\alpha}^{(N)}(x,y)\, dx\, dy \tag{29}$$

Differentation matrices are useful in finite element analysis because they provide an exact numerical equivalent for the analytic process of differentiation of a finite element approximation. The equivalence is established by the following relation

$$\frac{\partial u(x,y)}{\partial x} = \frac{\partial \tilde{\alpha}^{(N)}(x,y)}{\partial x}\, \underset{\sim}{u} = \tilde{\alpha}^{(N-1)}(x,y) D_x\, \underset{\sim}{u} \tag{30}$$

where the matrix D_x is composed of a sum of the matrices $G^{(m)}$

$$D_x = \sum_m b_m G^{(m)} \tag{31}$$

and the b_m are determined from the element vertices.

It is important to notice two things about Equation 30. One is that no analytical operator appears on the right-hand-side of Equation 30; the other is that the polynomial order of the approximation is decreased by one by the process of differentiation. This latter fact implies further that the matrix D_x is rectangular in shape.

Since two orders of interpolation polynomials are involved in Equation 30, an apppoximate relationship between these two orders must be defined. Following reference 20, this relationship is provided by the projection operator P which minimizes the L_2 norm of the difference between the Nth order approximation $u^{(N)}(x,y) = \tilde{\alpha}^{(N)}(x,y)\, \underset{\sim}{u}$ and the (N-1)st order approximation $u^{(N-1)}(x,y) = \tilde{\alpha}^{(N-1)}(x,y)\, \underset{\sim}{u}$

$$\left\| u^{(N)}(x,y) - u^{(N-1)}(x,y) \right\| = \text{minimum} \tag{32}$$

The numerical equivalent of the projection operator P is given by the projection matrix P. The projection matrix satisfies the equation

$$P\, u^{(N)}(x,y) = P\, \tilde{\alpha}^{(N)}(x,y)\, \underset{\sim}{u} = \tilde{\alpha}^{(N-1)}(x,y)\, P\, \underset{\sim}{u} \tag{33}$$

As is the case with differentiation matrices D_x, the projection matrices P is a rectangular matrix.

6. EXAMPLE

Finite element discretization via the elementary matrix concept will now be illustrated. Consider the diffusion equation (15) in Cartesian coordinates

$$\frac{\partial^2 A_z}{\partial x^2} + \frac{\partial^2 A_z}{\partial y^2} = jkA_z \tag{34}$$

where $k = \omega\sigma\mu_r\mu_o$. For this equation, the Galerkin equation (21) is

$$\left(\int \tilde{\alpha}^T \frac{\partial^2 \tilde{\alpha}}{\partial x^2}\, dxdy + \int \tilde{\alpha}^T \frac{\partial^2 \tilde{\alpha}}{\partial y^2}\right) \underset{\sim}{u} = jk \int \tilde{\alpha}^T \tilde{\alpha}\, dxdy\, \underset{\sim}{u} \tag{35}$$

where we have set $A_z = \tilde{\alpha}(x,y)\, \underset{\sim}{u}$. Using Green's theorem, Equation 35 may be written as

$$S\, \underset{\sim}{u} = -jk\, T\, \underset{\sim}{u} \tag{36}$$

where

$$S = \int \left(\frac{\partial \tilde{\alpha}^T}{\partial x} \frac{\partial \tilde{\alpha}}{\partial x} + \frac{\partial \tilde{\alpha}^T}{\partial y} \frac{\partial \tilde{\alpha}}{\partial y}\right) dxdy$$
$$T = \int \tilde{\alpha}^T \alpha\, dxdy \tag{37}$$

The matrix T in Equation 36 is simply the elementary matrix $T^{(N)}$ of Equation 27; to evaluate the matrix S, substitute $\frac{\partial \tilde{\alpha}}{\partial x} = \tilde{\alpha}^{(N-1)} D_x$, $\frac{\partial \tilde{\alpha}}{\partial y} = \tilde{\alpha}^{(N-1)} D_y$ and use Equation 27 again.

The result is

$$S = D_x^T T^{(N-1)} D_x + D_y^T T^{(N-1)} D_y \tag{38}$$

This result is identical to that given by Silvester[2], although it is in a different form.

7. MAGNETIC FIELD FORMULATION

It is apparent from the literature survey presented in Sections 1 and 2 that all existing finite element solutions of time-varying magnetic field problems are based on a vector potential formulation of the magnetic field. The reason for this is that the vector potential reduces to a single component function in two-dimensional problems. This is not the case with three-dimensional problems, where, as demonstrated by Okuda, a four component vector formulation similar to that given in Equations 11 and 12 must be used. Therefore, in three-dimensional problems, no advantage is to be gained in working with the vector potential A instead of directly solving for the magnetic field vector B, since at least three field components exist in either case.

A magnetic field formulation of time-varying magnetic field problems is obtained by starting with the second Maxwell equation $\nabla \times \bar{H} = \bar{J}$ and substituting for $\bar{H}$ and $\bar{J}$ from Equation 6. Assuming low velocities, there results

$$\nabla \times \bar{B} = \sigma\mu_r\mu_o \bar{E} + \sigma\mu_r\mu_o (\bar{V}_m - \bar{V}_c) \times \bar{B} \tag{39}$$

Taking the curl of both sides of Equation 38 and using the first Maxwell equation yields

$$\nabla \times \nabla \times \bar{B} - \sigma\mu_r\mu_o (\bar{V}_m - \bar{V}_c) \times \bar{B} = -\sigma\mu_r\mu_o \frac{\partial \bar{B}}{\partial t} \tag{40}$$

Finally, noting that the divergence of $\bar{B}$ is zero, and assuming sinusoidal time variations, Equation 40 becomes

$$\nabla^2 \bar{B} + \sigma\mu_r\mu_o (\bar{V}_m - \bar{V}_c) \times \bar{B} = jk\bar{B} \tag{41}$$

where $k = \omega\sigma\mu_r\mu_o$. Equation 41, together with the divergence condition $\nabla \cdot \bar{B} = 0$, governs the behavior of the magnetic field in electric machines under time-harmonic conditions.

Equation 41 for the magnetic field fector $\bar{B}$ differs radically from the governing Equation 11 for the vector potential $\bar{A}$ because the three components of the vector $\bar{B}$ are not coupled as in Equation 41. Instead, the three components of the magnetic field $\bar{B}$ are coupled by the zero divergence condition on the field. Since finite element approximating functions do not satisfy the zero-divergence condition automatically, special finite element approximations must be developed to solve magnetic field problems using Equation 41.

8. APPROXIMATION OF NON-DIVERGENT VECTOR FIELDS

Although the magnetic field in Equation 41 in general has three non-zero components, in this paper only the simplified problem of approximating a two-dimensional, two component magnetic field vector $\bar{B}$ is presented. Since any function may be approximated by the finite element basis functions $\tilde{\alpha}(x,y)$, we may write

$$B_x = \tilde{\alpha}(x,y)\, \underset{\sim}{k}$$
$$B_y = \tilde{\alpha}(x,y)\, \underset{\sim}{p} \tag{42}$$

where the coefficients $\underset{\sim}{k}$ and $\underset{\sim}{p}$ are to be determined. Let us write two component vectors in the column form

$$\bar{B} = \begin{bmatrix} B_x \\ B_y \end{bmatrix} \tag{43}$$

The approximation given in Equation 42 may, therefore, be written in the vector form

$$\bar{B} = \begin{bmatrix} \tilde{\alpha}(x,y) \\ 0 \end{bmatrix} \underset{\sim}{k} + \begin{bmatrix} 0 \\ \tilde{\alpha}(x,y) \end{bmatrix} \underset{\sim}{p} \tag{44}$$

The coefficients $\underset{\sim}{k}$ and $\underset{\sim}{p}$ in Equation 44 are, of course, not all independent: they are inter-related by the fact that the vector $\bar{B}$ is non-divergent

$$\frac{\partial \tilde{\alpha}(x,y)}{\partial x} \underset{\sim}{k} + \frac{\partial \tilde{\alpha}(x,y)}{\partial y} \underset{\sim}{p} = 0 \tag{45}$$

Using Equation 30, Equation 45 becomes

$$\tilde{\alpha}^{(N-1)}(x,y)\, D_x \underset{\sim}{k} = - \tilde{\alpha}^{(N-1)}(x,y)\, D_y \underset{\sim}{p} \tag{46}$$

Equation 46 states the conditions on the approximation in Equation 44 for this approximation to have exactly zero divergence at every point. However, in magnetic field problems, we are interested in determining solutions which satisfy all three of the following conditions:

(i) The solution must be non-divergent;

(ii) The solution must satisfy Equation 41;

(iii) The solution must satisfy the boundary conditions.

If Equation 45 is imposed exactly then condition (i) is satisfied exactly, but conditions (ii) and (iii) are satisfied only crudely. With numerical solutions, it is better to approximate each requirement equally, so that convergence to all conditions is of the same order of magnitude. In the present case, if we impose condition (i) only approximately, a greater number of degrees of freedom on the finite element solution are available to satisfy conditions (ii) and (iii). The zero-divergence of the magnetic field is approximated in this paper by projecting both sides of Equation 45 onto a lower-order function space. The matrix equation which results from the projection is

$$P\, D_x \underset{\sim}{k} = - P\, D_y \underset{\sim}{p} \tag{47}$$

This matrix equation is singular, since both matrices $P\, D_x$ and $P\, D_y$ are rectangular. It is therefore only possible to solve Equation 47 for $\underset{\sim}{k}$ and $\underset{\sim}{p}$ by using the concept of matrix generalized inversion[21,22]. According to this theory, the general solution of Equation 46 is given by

$$\underset{\sim}{k} = - (P\, D_x)^+ P\, D_y \underset{\sim}{p} + N_x \underset{\sim}{q} \tag{48}$$

or

$$\underset{\sim}{p} = - (P\, D_y)^+ P\, D_x \underset{\sim}{k} + N_y \underset{\sim}{\ell} \tag{49}$$

where $(P\, D_x)^+$ and $(P\, D_y)^+$ are the generalized inverses of $P\, D_x$ and $P\, D_y$, respectively. N_x and N_y are the nullmatrices of $P\, D_x$ and $P\, D_y$, respectively, and the vectors $\underset{\sim}{q}$ and $\underset{\sim}{\ell}$ are arbitrary.

Substituting Equations 48 and 49 into Equation 44 gives

$$\bar{B} = \begin{bmatrix} \tilde{\alpha}(x,y) \\ -\tilde{\alpha}(x,y) R_y \end{bmatrix} \underset{\sim}{k} + \begin{bmatrix} 0 \\ \tilde{\alpha}(x,y) N_y \end{bmatrix} \underset{\sim}{\ell} \tag{50}$$

or

$$\bar{B} = \begin{bmatrix} -\tilde{\alpha}(x,y) R_x \\ \tilde{\alpha}(x,y) \end{bmatrix} \underset{\sim}{p} + \begin{bmatrix} \tilde{\alpha}(x,y) N_x \\ 0 \end{bmatrix} \underset{\sim}{q} \tag{51}$$

where

$$\begin{aligned} R_y &= (P\, D_y)^+ P\, D_x \\ R_x &= (P\, D_x)^+ P\, D_y \end{aligned} \tag{52}$$

Equations 50 and 51 are interpreted in the following way: If a finite element approximation is made to one component (either $B_x = \tilde{\alpha} \underset{\sim}{k}$ or $B_y = \tilde{\alpha} \underset{\sim}{p}$) of a two component non-divergent vector, then the other component consists of two parts: One part of the second component (either $-\tilde{\alpha} R_y \underset{\sim}{k}$ or $-\tilde{\alpha} R_x \underset{\sim}{p}$) contains those functions which form a non-divergent pair with the first component. The second part of the approximation (either $\tilde{\alpha} N_y \underset{\sim}{\ell}$ or $\tilde{\alpha} N_x \underset{\sim}{q}$) provides those functions which are required to make the approximation of the second component complete in the vector space, but for which no corresponding term in the first approximation exists.

It is important to recognize that while the basis vectors for $\bar{B}$ in Equation 50 or in Equation 51 form a complete interpolatory set for one component of $\bar{B}$, they do not form a complete interpolatory set for the second component. Although it is possible to make two different complete interpolatory approximations for B_x and for B_y, as is given in Equation 42, these two approximations are not independent. To obtain a set of basis functions in a non-divergent vector space, one may take either the approximation

for B_x or the approximation for B_y to be interpolatory; the approximation for the second component is not interpolatory and is, in fact, related to the interpolatory basis through equations 48 and 49.

Finally, Equations 48 and 49 can be combined to yield two direct relationships between the four coefficients $\underset{\sim}{p}$ and $\underset{\sim}{\ell}$, and $\underset{\sim}{k}$ and $\underset{\sim}{q}$.

First, however, note that if a matrix A is of full row rank, the matrix A, its generalized inverse A^+, and its nullmatrix N satisfy the following properties[22]

$$\begin{aligned} A\,A^+ &= I \\ A\,N &= 0 \end{aligned} \tag{53}$$

Using Equation 53 and substituting $\underset{\sim}{k}$ from Equation 48 into Equation 49 gives

$$N_y \underset{\sim}{\ell} = (I - (P\,D_y)^+ P\,D_y)\,\underset{\sim}{p} \tag{54}$$

Similarly, substituting $\underset{\sim}{p}$ from Equation 49 into Equation 48 gives

$$N_x \underset{\sim}{q} = (I - (P\,D_x)^+ P\,D_x)\,\underset{\sim}{k} \tag{55}$$

It is well known[22] that the matrix $(I - A^+A)$ provides the orthogonal projector onto the nullspace of the matrix A. Therefore, Equations 54 and 55 state that the quantities $N_y\underset{\sim}{\ell}$ or $N_x\underset{\sim}{q}$ are obtained by projecting the original approximation for the opposite component onto the nullspace of the operators $P\,D_y$ or $P\,D_x$.

9. VARIATIONAL FORMULATION

Equation 41, which governs the behavior of time-harmonic magnetic fields, is solved by using the non-divergent approximation vectors in Equations 50 and 51 as follows:

Setting $\overline{V}_m = \overline{V}_c$ and assuming that $B_z = 0$, Equation 41 may be written in the matrix form

$$\begin{bmatrix} \nabla^2 - jk & 0 \\ 0 & \nabla^2 - jk \end{bmatrix} \begin{bmatrix} B_x \\ B_y \end{bmatrix} = \begin{bmatrix} 0 \\ 0 \end{bmatrix} \tag{56}$$

Furthermore, the non-divergent approximation for the vector $\overline{B}$ in Equation 50 may be written as

$$\begin{bmatrix} B_x \\ B_y \end{bmatrix} = \begin{bmatrix} \underset{\sim}{\alpha}(x,y) & \\ & \underset{\sim}{\alpha}(x,y) \end{bmatrix} \begin{bmatrix} I & 0 \\ -R_y & N_y \end{bmatrix} \begin{bmatrix} \underset{\sim}{k} \\ \underset{\sim}{\ell} \end{bmatrix} \tag{57}$$

Therefore, the Galerkin equations for Equation 56 are given by

$$\int \begin{bmatrix} I & R_y^T \\ 0 & N_y^T \end{bmatrix} \begin{bmatrix} \underset{\sim}{\alpha}^T & \\ & \underset{\sim}{\alpha}^T \end{bmatrix} \begin{bmatrix} \nabla^2 - jk & 0 \\ 0 & \nabla^2 - jk \end{bmatrix} \begin{bmatrix} I & 0 \\ -R_y & N_y \end{bmatrix} \begin{bmatrix} \underset{\sim}{\alpha} & \\ & \underset{\sim}{\alpha} \end{bmatrix} \begin{bmatrix} \underset{\sim}{k} \\ \underset{\sim}{\ell} \end{bmatrix} = 0 \tag{58}$$

Expanding this result and noting the fact that $S = -\int \underset{\sim}{\alpha}^T \nabla^2 \underset{\sim}{\alpha}\,dxdy$ gives

$$A\,\psi = -\,jk\,T\,\psi \tag{59}$$

where

$$A = \begin{bmatrix} S + R_y^T S R_y & -R_y^T S N_y \\ -N_y^T S R_y & N_y^T S N_y \end{bmatrix}$$

$$B = \begin{bmatrix} T + R_y^T T R_y & -R_y^T T N_y \\ -N_y^T T R_y & N_y^T S N_y \end{bmatrix} \tag{60}$$

$$\psi = \begin{bmatrix} \underset{\sim}{k} \\ \underset{\sim}{\ell} \end{bmatrix}$$

Equation 59 can be solved for the unknowns $\underset{\sim}{k}$ and $\underset{\sim}{\ell}$; the coefficients $\underset{\sim}{p}$, which provide interpolative values for B_y are determined by using Equation 49.

10. CONCLUSION

All finite element solutions of magnetic field problems appearing in the literature today are based on a vector potential formulation of the magnetic field. In these solutions, the magnetic field is determined indirectly by solving the relevant field equation for the vector potential, and then taking the curl of the vector potential to yield the magnetic field. Five different types of field problems have been solved: magnetostatic field problems, eddy-current problems, skin-effect problems, moving-body problems, and transient field problems; all of these different problems may be viewed as special cases of a general time-varying magnetic field formulation.

Magnetic vector potential formulations of two-dimensional problems are especially simple, because in these cases, the vector potential reduces to a single component vector and automatically satisfies the zero-divergence condition. In three-dimensional problems, however, the vector potential formulation is considerably more complicated: not only does the vector potential have three non-zero components in three-dimensions, but the divergence of the vector potential is, in general, not equal to zero. Indeed, in three-dimensions, the divergence of the vector potential is proportional to the Laplacian of the magnetic scalar potential, and the magnetic field problem must be solved as a coupled system of four equations and four unknowns.

An alternative to the four component vector potential formulation of three-dimensional magnetic field problems is to solve for the magnetic field directly in terms of its three field components. In this formulation, the magnetic field equation reduces to a set of three independent field equations, one for each of the three field components. However, since the divergence of the magnetic field must always equal zero, the three magnetic field components are not, in fact, independent.

Numerical conditions for approximating two-dimensional non-divergent vector fields are investigated in this paper. The procedures developed are based on the use of elementary differentiation and projection matrices to replace the processes of differentiation and approximation on finite element functions. It is shown that it is not possible to approximate the two components of a two-dimensional non-divergent vector field with two independent finite element functions. To obtain a set of basis functions in a non-divergent vector space, either component may be taken as interpolatory; the other component is related to it in a simple way.

The ideas developed in this paper are being investigated further to determine their utility; the results of this investigation will be reported shortly.

11. REFERENCES

1. Silvester, P., and Chari, M.V.K., "Finite-Element Solution of Saturable Magnetic Field Problems", IEEE Trans. on Power App. and Syst., Vol. PAS-89, 1970, pp. 1642-1651.

2. Silvester, P., and Haslam, C.R.S., "Magnetotelluric Modeling by the Finite Element Method", Geophysical Prospecting, Volume 20, 1972, pp. 872-891.

3. Chari, M.V.K., "Finite Element Solution of the Eddy-Current Problem in Magnetic Structures", IEEE Trans. on PAS, Volume PAS-93, 1974, pp. 62-72.

4. Donea, J., Guiliani, S., and Philippe, A., "Finite Elements in the Solution of Electromagnetic Induction Problems", Int. J. Numerical Methods in Engineering, Volume 8, 1974, pp. 359-367.

5. Carpenter, C.J., "Finite Element Network Models and Their Application to Eddy Current Problems", Proc. IEE, Vol. 122, 1975, pp. 455-461.

6. Sato, T., Suzuki, Y., Saito, S., and Inui, Y., "Calculation of Magnetic Field Taking Into Account Eddy Current and Nonlinear Magnetism", Denki Gakkai Ronbrushki, Volume 96B, 1976, pp. 399-405 (translated in Electrical Eng. in Japan, Volume 96, 1976, pp. 96-102).

7. Brauer, J.R., "Finite Element Analysis of Electromagnetic Induction in Transformers", IEEE PES Winter Power Meeting, 1977, paper.

8. Csendes, Z.J., and Chari, M.V.K., "Finite Element Analysis of Eddy Current Effects in Rotating Electric Machines", IEEE PES Summer Meeting, 1977, paper A 77 615-8.

9. Chari, M.V.K., and Csendes, Z.J., "Finite Element Analysis of the Skin Effect in Current Carrying Conductors", IEEE Trans., Volume MAG-13, 1977, pp. 1125-1127.

10. Konrad, A., Coulomb, J.L., Sabonnadiere, S.C., and Silvester, P.P., "Finite Element Analysis of Steady-State Skin Effect in a Slot-Embedded Conductor", IEEE PES Winter Meeting, 1976, paper A 76-189-1.

11. Foggia, A., Sabonnadiere, J.C., and Silvester, P., "Finite Element Solution of Saturated Travelling Magnetic Field Problems", IEEE Trans. on PAS, Volume PAS-94, 1975, pp. 866-871.

12. Hannalla, A.Y., and Macdonald, D.C., "Numerical Analysis of Transient Field Problems in Electrical Machines", Proc. IEEE, Volume 123, 1976, pp. 893-898.

13. Yamada, S., Kanamaru, Y., and Besalo, K., "The Transient Magnetization Process and Operations in the Plunger Type Electromagnetic", IEEE Trans., Volume MAG-12, 1976, pp. 1056-1058.

14. Demerdash, N.A., and Lau, N.K., "Flux Penetration and Losses in Solid Nonlinear Ferromagnetics using Space Techniques Applied to Electrical Machines", IEEE Trans. Volume MAG-12, 1976, pp. 1039-1041.

15. Okuda, H., "Finite Element Solution of Travelling Wave Magnetic Field and Eddy Current", Electrical Eng. in Japan, Volume 96, 1976, pp. 75-82.

16. Becker, E.B., Pillsbury, R.D., Driga, M.D., "Magnetic Field Diffusion in Fast Discharging Homopolar Machines: A Finite Element Approach", Compumag Conference Proceedings, Oxford, 1976, pp. 417-422.

17. Shiozawa, T., "Phenomenological and Electron-theoretical Study of the Electrodynamics of Rotating Systems", Proc. IEEE, Volume 61, pp. 1694-1703, 1973.

18. Babuska, I., Prager, M., and Vitasek, E, Numerical Processes in Differential Equations, New York, Interscience, 1966.

19. Csendes, Z.J., Gopinath, A., and Silvester, P., "Generalized Matrix Inverse Techniques for Local Approximations of Operator Equations", The Mathematics of Finite Elements and Applications, London: Academic Press, 1973, pp. 189-199.

20. Csendes, Z.J., "A Finite Element Method for the General Solution of Ordinary Differential Equations", Int. J. for Numerical Methods in Engineering, Volume 9, 1975, pp. 551-561.

21. Silvester, P., "Construction of Triangular Finite Element Universal Matrices", Int. J. for Numerical Methods in Engineering, Volume 12, 1978, pp. 237-244.

LAYER THEORY ANALYSIS FOR INTEGRAL-BAR INDUCTION DEVICES

S. Williamson and A. C. Smith
Department of Engineering, University of Aberdeen, Aberdeen, U.K.

ABSTRACT

This paper is a preliminary report of a development of layer theory which takes the discrete nature of the rotor currents into account, and which is therefore applicable to the vast majority of rotating induction machines. The analysis is verified by comparison with the equivalent circuit method.

1. INTRODUCTION

The analysis of induction machines using a multilayer model has gained favour with the rise of research activity in the field of linear motors. This may be attributed to two factors. Firstly, there is an obvious physical similarity between the linear motor and the idealised layer theory model, and secondly conventional equivalent circuit techniques have proved unable to model the linear motor accurately. In addition, layer theory has the inherent ability to incorporate the unbalanced electric conditions that prevail in the linear motor, and being a field solution technique it will yield the field distribution in the airgap for a little extra computational effort.

The normal layer theory approach models the rotor conduction layer by a homogeneous conducting sheet. In a linear motor this involves no approximation, since these devices almost invariably employ sheet secondaries. The vast majority of induction machines, however, have cage rotors which consist of discrete bars housed in slots in the rotor surface. Furthermore, the rotor cage is frequently skewed, so that the rotor bar currents are constrained to flow in strictly non-axial paths. Both of these aspects introduce features which cannot be included in a homogeneous-rotor model. The discrete bar currents produce slot-harmonic fields which can constitute a significant part of the rotor leakage. These are not present in the normal model. Similarly, there is no mechanism in the homogeneous rotor model for constraining the rotor currents to flow in non-axial paths, so that the axial flux variations produced by skewing cannot be examined. It is not surprising, therefore, that layer theory has not found widespread use for the analysis of rotating induction machines.

This paper introduces a new form of layer theory which enables the rotor currents to flow in discrete paths, and which is therefore applicable to rotating induction motors. The analysis is developed in a form appropriate to cage rotor machines, although, with a few minor modifications it is equally applicable to wound-rotor machines.

2. THEORETICAL DEVELOPMENT

2.1 Sheet Rotor Layer Theory

Many of the features of discrete-bar layer theory are essentially similar to those of the usual 'sheet rotor' version, and it is therefore appropriate to begin the development with a brief account of the latter. Full accounts may be found in references 1-3.

The machine is modelled by a series of parallel (or concentric) regions, as shown in fig. 1. Each region is characterised by its position, thickness, and material constants, which are empiracally derived from the part of the machine that the region represents. The regions may be isotropic or anisotropic[3,4], but are assumed to be both homogeneous and linear.

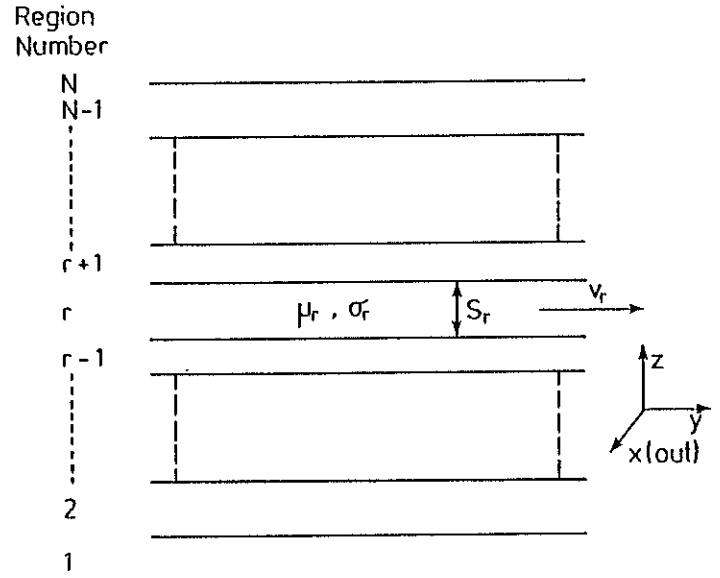

figure 1 General layer theory model.

The analysis is quasi-two dimensional: it is assumed that no quantities vary in the transverse (x) direction, and the use of harmonic analysis and the principle of superposition allow the longitudinal (y-directed) variations to be accounted for. Variation of fields in the z-direction can therefore be determined for each longitudinal harmonic. It is assumed, here, that the sinusoidal steady-state prevails, so that the $j\omega$ operator may be used to advantage. Each region is allowed to move in the y-direction with a

velocity which may differ from all the other regions. This allows the relative motion between the rotor and stator to be taken into account.

For a general region (the r^{th}) and a general wave number k, it is relatively simple to show that the electric and magnetic field strengths measured within the region in a reference frame that is attached to it, are given by

$$\begin{aligned}
\bar{H}_x^k &= 0 \\
\bar{H}_y^k &= \gamma(C \sinh\gamma z + D \cosh\gamma z)e^{j(s_k\omega t - ky)} \\
\bar{H}_z^k &= jk(C \cosh\gamma z + D \sinh\gamma z)e^{j(s_k\omega t - ky)} \qquad (1) \\
\bar{E}_x^k &= \frac{-s_k\omega\mu}{k}\bar{H}_z \\
\bar{E}_y^k &= \bar{E}_z^k = 0
\end{aligned}$$

where s_k is the fractional slip of the r^{th} region with respect to the stationary reference frame - usually the stator - for the wave number k

$$s_k = 1 - \frac{v_r k}{\omega} \qquad (2)$$

and

$$\gamma^2 = k^2 + js_k\omega\mu\sigma \qquad (3)$$

The constants of integration in equations (1) may be expressed in terms of the field values at the region boundaries, but a more convenient formulation employs the transfer matrix concept, thus

$$\begin{bmatrix} \bar{B}_r^k \\ \bar{H}_r^k \end{bmatrix} = \begin{bmatrix} \cosh\gamma S_r & \frac{jk\mu}{\gamma}\sinh\gamma S_r \\ \frac{\gamma}{jk\mu}\sinh\gamma S_r & \cosh\gamma S_r \end{bmatrix} \begin{bmatrix} \bar{B}_{r-1}^k \\ \bar{H}_{r-1}^k \end{bmatrix} \qquad (4)$$

$\bar{B}_r^k$ is an abreviated notation for the value of $\bar{B}_z^k$ at the upper boundary of region r and $\bar{B}_{r-1}^k$ is the value of the same field component at the lower boundary of region r. Similarly, $\bar{H}_r^k$ and $\bar{H}_{r-1}^k$ refer to $\bar{H}_y^k$ at the corresponding boundaries. Continuity conditions dictate that $\bar{B}_z^k$ and $\bar{H}_y^k$ should be invariable across the region boundaries, so that their explicit calculation at any one boundary allows their calculation at all other boundaries, and hence the solution of the field inside any region is possible, if required. The field values at the boundary surfaces of the excitation layer when just one winding is excited can be calculated directly from the current density produced by the excitation, after an intermediate calculation of winding surface impedances, which are derivable from the transfer matrices[2].

The boundary field values are subsequently used for the calculation of coupling impedances between the excited stator winding and all other stator windings, which are temporarily assumed to be open-circuited for this purpose. The harmonic components are summed and winding resistances and external impedances are added, until, finally a matrix of coupling impedances is obtained.

$$\begin{bmatrix} \bar{V}_{S1} \\ \bar{V}_{S2} \\ \bar{V}_{S3} \end{bmatrix} = \begin{bmatrix} \bar{Z}_{S1,S1} & \bar{Z}_{S1,S2} & \bar{Z}_{S1,S3} \\ \bar{Z}_{S2,S1} & \bar{Z}_{S2,S2} & \bar{Z}_{S2,S3} \\ \bar{Z}_{S3,S1} & \bar{Z}_{S3,S2} & \bar{Z}_{S3,S3} \end{bmatrix} \begin{bmatrix} \bar{I}_{S1} \\ \bar{I}_{S2} \\ \bar{I}_{S3} \end{bmatrix} \qquad (5)$$

It has been assumed that there are three separate stator windings, but it will be appreciated that the impedance matrix will be of dimension M, equal to the number of independent stator windings. Solution of equation (5) for the winding currents is a routine matter, and the total field at any point in the machine may subsequently be determined by substituting back into the original equations.

It must be emphasised, here, that the rotor layer is treated like any other non-excitation layer, so that the rotor currents need not be calculated explicitly.

2.2 Discrete Bar Layer Theory

In the discrete bar layer theory the rotor is regarded as constituting an excitation layer, which is eventually short-circuited when the final impedance matrix is assembled.

The solution begins, as before, with the calculation of the stator-stator coupling impedances, with the essential difference that the

conductivity of the rotor layer is set to zero, although eddy currents are allowed to flow in any other non-excitation layer, as appropriate.

The emf induced in the rotor when a stator winding is excited is used to define stator-rotor coupling impedances. The response of the rotor differs between space harmonics, so that it is necessary to calculate stator-rotor coupling impedances for each harmonic independently, and these may not be summed in the way that the stator-stator impedances may. The emfs induced in the rotor bars by a stator-driven field of wave number k have a fixed amplitude but a phase progression of $k\lambda$ radians, where λ is the rotor slot pitch. The response of the whole rotor cage to a particular wave can therefore be typified by a single bar, which may be positioned conveniently at the origin of the rotor reference frame. The emf induced in this bar, which is assumed to be rectangular, of depth d and breadth b, can be shown to be given by

$$\bar{U}^k = s_k w K_{dk} K_{bk} \left[\frac{\bar{E}^k_m + \bar{E}^k_{m-1}}{2}\right] e^{js_k\omega t} \qquad (6)$$

where w is the bar length, m is the reference number for the rotor bar layer, and K_{dk} and K_{bk} are depth and width factors for the bar.

$$K_{dk} = \frac{\tanh(\frac{kd}{2})}{(\frac{kd}{2})} \qquad K_{bk} = \frac{\sin(\frac{kb}{2})}{(\frac{kb}{2})} \qquad (7)$$

$\bar{E}^k_m$ is the value of $\bar{E}^k_x$ at the top surface of the rotor bar layer, and $\bar{E}^k_{m-1}$ is the value at the lower surface. These may be calculated from $\bar{B}^k_z$ at the corresponding positions using the standard layer theory techniques described in the previous section. The ratio of $\bar{U}^k$ to the winding current then defines the coupling impedance between the reference rotor bar and the current in the excited winding, for a wave of number k.

The harmonic emfs induced in the rotor bars drive rotor currents with the same spatial phase distribution and of the same frequency as the induced emfs. The next step is to determine the coupling impedance between these current distributions and the stator windings and with themselves. This is done by assuming the rotor carries a current distribution of the form prescribed for, say, the k^{th} harmonic. As before this can be characterised by the current $\bar{I}^k$ flowing in the reference bar. Fourier analysis is used to convert these discrete bar currents into an equivalent sum of current density distributions.

$$\bar{J}^k = \frac{\bar{I}^k}{d\lambda} \sum_{n=-\infty}^{+\infty} K_{b\ell} e^{j(s_k\omega t - \ell y)} \qquad (8)$$

where $K_{b\ell}$ is defined in equation (7), and ℓ is related to the summation index n by

$$\ell = k + n\left[\frac{2\pi}{\lambda}\right] \qquad (9)$$

The value $n = 0$ produces $\ell = k$, showing that this current density wave has the same distribution as the inducing wave. This may be called the principal current density wave for the k^{th} harmonic. Other values of n produce $\ell \neq k$, which signifies current density waves of one wave number (ℓ) with a speed of rotation not appropriate to that harmonic. These are the rotor slot harmonics for the k^{th} wave, and their significance is that they tend to induce non-mains frequency emfs in the stator windings, although they induce emfs of the same frequency and distribution as the parent bar currents in the rotor cage. Their effect on the stator is usually small enough to be neglected, and this will be assumed to be the case in this instance, but they can contribute a significant part of the (leakage) impedance of the rotor cage. It is these slot harmoncis which are neglected in the sheet rotor model.

Having resolved the bar currents into harmonic spectra, the conventional layer theory approach may be used to determine coupling impedances with the stator winding (n=0, only) and the rotor reference bar (all values of n). The latter involves a summation over all the rotor slot harmonics, to give a single impedance component.

The coupling impedances are finally assembled into an impedance matrix, which takes the form illustrated in fig. 2. The first subscript, S, refers to the stator, whilst the second, R, refers to the rotor. The second stator subscript indicates the stator phase number, whilst the second rotor subscript refers to the rotor bar harmonic current number. For example, $\bar{Z}_{Rn,Sm}$ indicates that when stator winding m carries a current of $\bar{I}_m$ amps, the n^{th} harmonic emf induced in the rotor reference bar will be $\bar{I}_m \bar{Z}_{Rn,Sm}$ volts. The impedance matrix dimension is now M + N, equal to the number of independent stator windings (M) plus the number of harmonics considered in the analysis (N). For clarity M=3 in fig. 2.

The external impedance components must now be added to the internal coupling components in the impedance matrix, and the matrix equation solved for the winding and harmonic bar currents. These may now in turn be inserted back into the layer model, so that field distributions may be calculated as required.

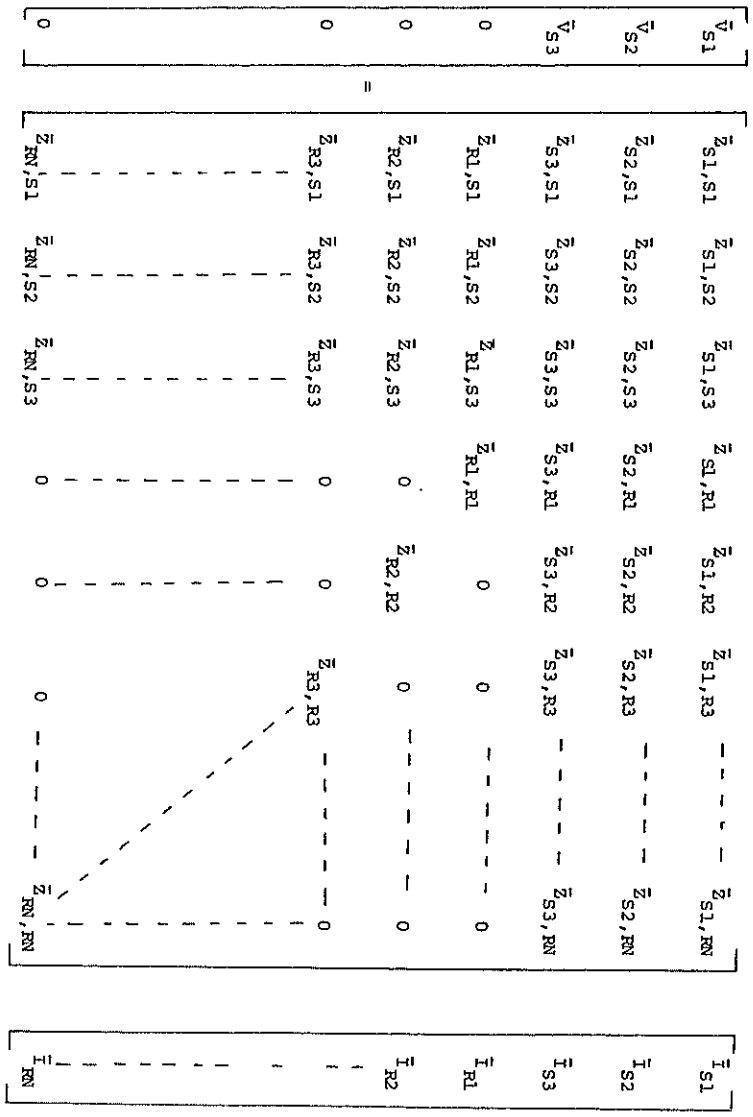

figure 2 Impedance matrix for discrete-bar rotor

3. VERIFICATION

The initial verification of this analysis was by comparison with the more usual equivalent circuit approach, to be found in most standard electrical machines texts. A worked design example by Say[6], for a 5kW, 415V, 3-phase, 50Hz, 4-pole cage motor gave values for the equivalent circuit components as well as the lamination and winding details. The data for this motor was input to a computer program for the discrete bar analysis which was used to predict the variation of torque, speed and input power with speed. These predictions were compared with those obtained using the equivalent circuit method, and were found to be indistinguishable.

The experimental verification of the analysis is currently being undertaken at Aberdeen University.

4. CONCLUSIONS

A form of layer theory has been developed which is capable of taking the discrete nature of the current flow paths in a rotating induction motor into account. The theory has proved to be comparable with the equivalent circuit approach for the analysis of a balanced three phase motor, but has the added advantage that unbalanced electrical conditions can equally well be taken into account. Its use will free the analyst from some of the more esoteric calculations of reactance and resistance components for use in a conventional equivalent circuit model.

5. REFERENCES

1. Greig, J., and Freeman, E.M.: Travelling-wave problem in electrical machines. Proc. IEE, Vol. 114, No. 11, pp 1681-1683

2. Freeman, E.M.: Travelling waves in induction machines: input impedance and equivalent circuits. Proc. IEE, Vol. 115, No. 12, pp 1772-1776, 1968

3. Freeman, E.M.: Computer aided steady state and transient solutions of quasi-one dimensional problems in induction devices. Proc. COMPUMAG Conf. on the Computation of Magnetic Fields, Oxford, April 1976

4. Williamson, S.: The anisotropic layer theory of induction machines and induction devices. J. Inst. Maths. Applics., Vol. 17, No. 1, pp 69-84, 1976

5. Williamson, S.: Induction motor analysis and field calculation using anisotropic layer theory. Proc. COMPUMAG Conf. on the Computation of Magnetic Fields, Oxford, April 1976

6. Say, M.G.: Alternating current machines. Pitman, London 1976

SURFACE ELEMENT MODELS OF CONDUCTING PLATES

C.J. Carpenter* and K.O. Sharples**

* Electrical Engineering Department, Imperial College, London SW7 2BT
** Electrical Engineering Department, City University, London EC1V 4PB

ABSTRACT

The limited depth of penetration of alternating fields into large conducting plates, and the correspondingly large field gradients, make it necessary to use small mesh intervals when computing the interior field numerically. This is commonly avoided by surface-element models which depend on the assumption that the penetration depth is small compared with the plate thickness. The flux in the conductor, and the currents induced, then depend only on the tangential field at the surface. When the plate is sufficiently thin, on the other hand, the induced currents depend only on the normal component of the incident flux, and limit the penetration depth in from the edge instead of in from the surface.

Both modes of penetration are combined in plates whose thickness falls between the two extremes. A more general form of surface-element model is described in which the nodes are confined to the conductor surface, but both normal and tangential fluxes are represented inside. Thick and thin plates are modelled as limiting examples. The paper gives details of the results obtained by applying the method to conducting plates subjected to a uniform incident field. The flux and loss distributions are compared with those computed numerically by placing sufficient nodes in the plate to obtain an accurate description of the field conditions.

The model is well suited to three-dimensional problems since only the external field is computed, and the equations are therefore derived in terms of magnetic scalar potential. The magnetic vector-potential formulation for two-dimensional transverse-magnetic geometries can be derived by duality.

1. INTRODUCTION

It is typical of many eddy current problems, particularly in large electrical machines and the like, that the depth of penetration in some, or all, of the conductors is small compared with the principal conductor dimensions. Under these conditions it is commonly assumed that the variations in the field quantities inside the conductors is sufficiently dominated by the gradient in the direction normal to the surface to make the interior solution approximately one-dimensional. The exterior field then "looks into" an equivalent surface impedance which can be calculated by solving the field equations in a semi-infinite block. This approximation makes it possible to avoid interior nodes, and confine the conductor description to surface elements, in a finite-element model, or the equivalent in finite-difference terms. The simplification is, of course, particularly important when the penetration depth is small, since a numerical solution inside the conductor demands correspondingly small elements, and hence large numbers of them.

Surface element models have been shown to work well in regions in which the tangential field gradients are sufficiently small. But they are less satisfactory near corners, particularly when these form junctions with secondary surfaces of smaller dimensions, and methods of modelling corners with better accuracy are under examination. The most important single example is a conducting plate whose major surfaces are large, relative to the penetration depth, but whose thickness is not, and it is the study of this particular configuration which is reported here. The thickness commonly exceeds a penetration depth, but may not be sufficient to prevent some interaction between the two surfaces. Moreover, detailed numerical solutions show a significant penetration of normal flux right through plates of moderate thickness, in a manner entirely inconsistent with a simple surface-element model. The additional flux may greatly affect the loss distribution, which is commonly concentrated near the edge.

The objective is to find a discrete model of the plate in which the nodes are confined to the surfaces, but which gives good accuracy for node spacings greater than a depth of penetration, d, defined by

$$1/d^2 = \omega\sigma\mu_o\mu$$

where ω is the angular frequency, σ the conductivity, and μ the permeability. The method applies to arbitrary waveforms, and to transients (both directly and by Fourier transform), but it is convenient to assume sinusoidal time variations, and hence linear material. Although saturation is of considerable practical importance it is the problem of modelling the geometric properties which is here of principal interest.

One advantage of surface-element models is that the magnetic scalar potential formulation of eddy-current problems[1] becomes particularly simple. The difficulties associated with the magnetic vector potential[2] are avoided, and three-dimensional solutions are straightforward, requiring no more than the appropriate increase in the number of nodes[3]. Here the mixed T-Ω formulation[1,2] is used inside the conductor, and is found to be particularly convenient for deriving the more general form of surface-node model. It reduces to the simple scalar (Ω) description of the external field.

2. MODES OF PENETRATION

The classical one-dimensional theory of flux penetration into a conductor assumes that the field is confined to the tangential direction, and the surface-element model likewise relates the eddy current loss to the tangential component of the flux density. The normal component is ignored, except for the implicit requirement that the continuity condition,

$$\text{div } B = 0$$

is satisfied in regions in which the tangential component is changing. This is in direct contrast to the behaviour of a plate, or lamination, which is so thin that the tangential field induces no significant amount of current. The eddy-current behaviour is then described entirely in terms of the normal component of flux density, and the tangential component is ignored. This thin-plate-type of response is specifically anisotropic, as can be seen by considering a stack of such plates, as in a laminated steel core, in which the flux directed in the plane of the laminations induces no current, whereas the response to normal fluxes is essentially that of a solid[4].

The different types of response of thick and thin conductors leads to the concept of two different modes of flux penetration occuring simultaneously in plates of moderate thickness, such as that illustrated in Fig. 1. Whereas the tangential, or x,y, components of the flux density penetrate in from the x,y surfaces, the normal, or z component, penetrates in from the edge. This simple picture is useful in gaining a qualitative understanding of the behaviour of a conductor which is plate-like in shape (i.e. with two dimensions much larger than the third). But it also provides the means for predicting the behaviour quantitatively, and the principal purpose of the paper is to describe how this can be done.

The qualitative picture shows at once a crucial difference in the nature of the two modes. Whereas the penetration of the tangential (x,y) components depends only on the material properties, in accordance with equation 1, the behaviour of the normal (z) component depends on the external conditions. This can be illustrated most simply by placing the plate in an air gap between two non-conducting iron surfaces distance g apart (Fig. 2). It can readily be shown that the propagation distance d', measured in the x direction from the plate edge, is

$$d' = d\sqrt{g/t} \qquad (2)$$

for the range of variables within which the field conditions are approximately one-dimensional in x. Thus we may expect a penetration depth substantially larger than d when the iron surfaces are removed altogether, or are relatively remote. This suggests that one way of utilising the nodal properties is to compute d' from equation 2, and combine the resulting behaviour with the thick-plate type of propagation mode from the surfaces, but this result is unnecessarily approximate, even when there are iron surfaces in close proximity. Having defined the plate in terms of nodes on the surface, the purpose of the numerical solution is to solve the external field, and, since it is the interaction of this with the conductor which determines d', it is clearly very desirable to make use of the information. To see how this can be done, it is helpful to consider first the problem of modelling a thin plate.

3. EQUATIONS FOR THIN PLATES

When the plate is sufficiently thin, so that there is no significant change in the internal field with z, and the internal tangential flux is negligible, only its electrical properties have to be taken

into account. The induced current can be described in terms of a current flow function, defined so that its gradient gives the surface current density. Thus the value of the flow function at any point gives the total current in the sheet between the point and the sheet edge. It follows that the flow function is a measure of the m.m.f., and hence the magnitude of the external magnetic potential discontinuity at the sheet, so that it is denoted $\Delta\Omega$. It is this which describes the electrical conditions in the conductor[5].

The equations for a sheet in the x,y plane are given in reference 5. The induced currents are due to B_z and are given by

$$\partial^2(\Delta\Omega)/\partial x^2 + \partial^2(\Delta\Omega)/\partial y^2 \equiv \nabla^2_{x,y}(\Delta\Omega) = j\omega\sigma t B_z \qquad (3)$$

This has to be solved simultaneously with the flux continuity condition

$$\nabla^2_{x,y,z}\,\Omega = 0 \qquad (4)$$

at all external points, whilst the corresponding equation for nodes on the plate is derived from the continuity of Ω on one side with $(\Omega + \Delta\Omega)$ on the other. B_z in equation 3 is then computed from the potential gradient at the surface.

When the plate thickness is increased the effect of the two surfaces is to screen the interior from the tangential field, but not from B_z. The reduction in B_z at any point depends on the extent to which the m.m.f. due to the total current flowing between the point and the edge - i.e. $\Delta\Omega$ - opposes the applied H_z field. This suggests that $\Delta\Omega$ is also important in describing the response of thick plates, and should be taken into account in modelling the plate.

4. FIELD EQUATIONS IN PLATE OF ARBITRARY THICKNESS

The modal description can be expressed quantitatively in a plate which is not thin by replacing $\Delta\Omega$ by an electric vector potential, T, satisfying the condition

$$\text{curl } T = J \qquad (5)$$

The T function is thus the electrical analogue of the magnetic vector potential, A, but it is usually convenient to define it differently from A by choosing the gauge, or divergence, so as to limit the number of vector components[1,2]. To derive the mode equations the plate thickness, t, is assumed to be sufficiently small, compared with the other plate dimensions, to make the z component of the current density J negligible. The electric vector potential can then be limited to a single component in the z direction[1,2] and the electric and magnetic field conditions inside the conductor are described by two (three-dimensional) equations, one for T and the other for the magnetic scalar potential, Ω.

The equation for T is derived from Faraday's law,

$$\text{curl } E = -j\omega B \qquad (6)$$

Substituting from equation 5 and expanding $\nabla x \nabla x$ T in Cartesian co-ordinates gives

$$\nabla^2_{x,y} T = j\omega\sigma B_z \qquad (7)$$

with no term in $\partial/\partial z$, although T varies in the z direction. The flux density B is derived from

$$B = \mu_o \mu H$$

where

$$H = T - \text{grad } \Omega \qquad (8)$$

from equation 5, since

$$\text{curl } H = J \qquad (9)$$

Substituting in equation 7 and integrating both sides with respect to z, from one plate surface to the other, gives

$$\nabla^2_{x,y}(\Delta\Omega) = j(\Delta\Omega + \Omega_o - \Omega_t)/d^2 \qquad (10)$$

where Ω_o and Ω_t denote the magnetic potential values at the plate surfaces (Fig. 3), and

$$\Delta\Omega = \int_o^t T\, dz \qquad (11)$$

is numerically equal to the total current flowing between the line of integration and the edge of the plate.

Thus the total current flow function, $\Delta\Omega$, in a thick plate, satisfies the same differential equation (3) as in a current sheet if we replace B_z by

$$\bar{B}_z = \frac{1}{t}\int_o^t B_z\, dz \qquad (12)$$

Moreover, by substitution from equation 8, this average B_z value is obtained directly from the two potential values at the surface, together with $\Delta\Omega$, i.e.

$$\bar{B}_z = \mu\mu_o(\Delta\Omega + \Omega_o - \Omega_t)/t \qquad (13)$$

Thus $\bar{B}_z$ is easily computed, and equation 10 shows that it is this which determines the total current flowing in any part of the plate, and thus the m.m.f. opposing flux penetration from the edge.

Equation 13 shows that $\bar{B}_z$ is the value of B_z which would be observed in a hole if sufficient material were removed to eliminate the field variations with z.

Equations for Ω_o and Ω_t are obtained by integrating the magnetic continuity condition

$$\text{div } B = \partial B_x/\partial x + \partial B_y/\partial y + \partial B_z/\partial z = 0$$

in a similar manner between nodes o and t on the surfaces. This gives

$$\partial \Phi_x/\partial x + \partial \Phi_y/\partial y = B_{zo} - B_{zt} \qquad (14)$$

where

$$\Phi_x = \int_o^t B_x \, dz \qquad (15a)$$

$$\Phi_y = \int_o^t B_y \, dz \qquad (15b)$$

are the total fluxes, per unit length, in the two tangential directions. It is these which are given by the tangential flux penetration mode. We have to solve this mode in terms of the surface Ω values, and relate the two modes to the two surface values of B_z, denoted B_{zo} and B_{zt}, to complete the surface equations.

5. TANGENTIAL FLUX PENETRATION

No assumptions are needed to derive equation 10 other than the neglect of J_z, so that the edge-mode behaviour which has been described in terms of thin plates is remarkably general. It is only in analysing the flux penetration from the surfaces that we need to add the conventional assumption that the normal, or z, gradients of the field quantities predominate. The fluxes Φ_x and Φ_y can then be computed from the tangential field components at the two surfaces but, whereas it is usually assumed that the two surface layers are independent of each other, a more general model is needed here which takes account of the interaction.

The relationships required are given in the appendix. The flux in either tangential direction (x or y) can be separated into two components, one associated with the bottom, and one with the top, surface, giving four components in all, denoted Φ_{xo}, Φ_{xt}, Φ_{yo} and Φ_{yt}. In both the x and y directions, taken separately, the two components are related to the tangential H fields at the surfaces, taken in the relevant direction, by the equations

$$j\omega\Phi_o = Y_s H_o + Y_m H_t \qquad (16a)$$

$$j\omega\Phi_t = -Y_m H_o - Y_s H_t \qquad (16b)$$

where the suffices o and t refer to the surfaces. The coefficients

$$Y_s = (1 + j\alpha^2)/2\sigma d\alpha \qquad (17a)$$

$$Y_m = (-1 + j\alpha^2)/2\sigma d\alpha \qquad (17b)$$

represent magnetic field admittances, or electric field impedances, per unit surface area, one a self-admittance and the other a mutual, or transfer, admittance. α is given by

$$\alpha = \left[1 - \exp(-\sqrt{j}\, t/d)\right]/\left[1 + \exp(-\sqrt{j}\, t/d)\right] \sqrt{j} \qquad (18)$$

As the plate thickness increases Y_m tends to zero, but the modelling of thin plates needs closer examination as the magnitudes of the real parts of both Y_s and Y_m tend to $1/\sigma t$ when t is small. Because the two surface fields tend to the same value as t tends to zero, the contributions from the real parts of Y_s and Y_m cancel, and the resultant flux progressively diminishes in a thin plate. The imaginary parts then predominate, because of the similarity of sign. These tend to $j\omega\mu_o \mu t/4$ when t is sufficiently small, so that the tangential properties are correctly represented over the full range of t values.

6. SURFACE NODE EQUATIONS

The simplest way of combining the two aspects of the plate behaviour is to describe them in terms of the properties of the branches in an equivalent magnetic network, that is, a network representing electromagnetic behaviour in which the flow and potential quantities are both magnetic[6]. The node equations are then obtained merely by summing fluxes in the appropriate branches. A two-dimensional cross-section through a typical node pair of the required network is shown in Fig. 3. For simplicity of illustration only one external connection is shown to each surface node, but when using a triangular mesh each connection represents the array of branches representing the edges of the elements which join at the node[7]. The first-order surface elements derived from equation 16 can be represented by horizontal branches, and when the plate is sufficiently thick these branches model the plate in the usual way. The more important aspect is the addition of the vertical branch to account for the transfer of

flux through the plate. When t is small this branch dominates the network behaviour.

In general, the connections which are illustrated diagrammatically in Fig. 3 enforce compliance with equation 14, since Φ_o and Φ_t together represent the tangential flux in the plate. If the vertical branch is defined as an m.m.f. source $\Delta\Omega$ in series with the appropriate reluctance, then it carries a flux Φ satisfying equation 13; more specifically

$$\Phi = \bar{B}_z h_x h_y \tag{19}$$

where h_x and h_y denote the tangential node spacings. Thus, provided that $\Delta\Omega$ satisfies equation 10, the branch properly controls the amount of flux transferred through the plate (i.e. the mis-match between the fluxes incident at the top and bottom and the amount directly tangentially), and it also represents correctly the response of the plate to that flux. Provided that Φ_o and Φ_t satisfy equation 16, all the necessary conditions are satisfied, and summing the fluxes at the surface nodes give equations for Ω_o and Ω_t.

The details are best illustrated in terms of a specific node array. A rectangular mesh with node spacing h_z in the z direction is assumed, for simplicity, outside the plate, and the surface and surrounding nodes are numbered according to the scheme shown in Fig. 4. The equivalent branch elements are shown in Fig. 5. The flow quantities in the network are not flux, Φ, but $j\omega\Phi$, in order to represent the energy storage and energy dissipative properties correctly, and reluctance becomes the magnetic equivalent of capacitance[8,6]. The reluctance of the vertical branch 01 is, by inspection $t/\mu_o\mu h_x h_y$, and placing this in series with the appropriate m.m.f. source, denoted $\Delta\Omega_{01}$, gives a branch flux in accordance with equations 19 and 13. The model differs in this respect from that used for thin sheets[5], in which the reluctance tends to zero, the potential difference $\Omega_1 - \Omega_0$ tends to $\Delta\Omega_{01}$ and B_z has to be found from the external potential gradient, but the more general description in terms of two different sets of surface nodes is always valid provided only that the two sets are not allowed to coalesce. Equation 10 can then be expressed in terms of vertical branch quantities only. The result can be derived by inspection. It reduces to

$$\Delta\Omega_{01}(2/h_x^2+2/h_y^2+j/d^2) = (\Delta\Omega_{27} + \Delta\Omega_{49})/h_x^2 + (\Delta\Omega_{38} + \Delta\Omega_{510})/h_y^2 + (\Omega_1-\Omega_0)j/d^2 \tag{20}$$

in a three-dimensional array, and when there is no variation with y the relevant terms have merely to be omitted. This equation defines $\Delta\Omega_{01}$.

From equation 16a, the flux in a typical surface branch 02 is given by

$$j\omega\Phi_{02} = Y_s(\Omega_0 - \Omega_2)h_y/h_x + Y_m(\Omega_1 - \Omega_7)h_y/h_x \tag{21}$$

when the problem is three-dimensional, or by

$$j\omega\Phi_{02} = Y_s(\Omega_0 - \Omega_2)/h_x + Y_m(\Omega_1 - \Omega_0)/h_x \tag{22}$$

when it is two-dimensional in x and z. Thus the surface behaviour can be represented diagrammatically by the network branches shown in Fig. 5, in which the admittance is $Y_s h_y/h_x$, or Y_s/h_x, as appropriate, and the Y_m term is equivalent to a flux source in parallel. Summing the fluxes at node 0 in a two-dimensional mesh therefore gives the equation

$$(\Omega_2+\Omega_4-2\Omega_0)(h_z/2+Y_s/\mu_o\mu)/h_x + (\Omega_7+\Omega_9-2\Omega_1)Y_m/\mu_o\mu h_x + (\Omega_6-\Omega_0)h_x/h_z + (\Omega_1-\Omega_0-\Delta\Omega_{01})h_x/t = 0 \tag{23}$$

for Ω_0. The extension to three dimensions is obtained by using 21 instead of 22, and summing over more branches.

The equivalent network becomes planar in problems which are two-dimensional, transverse-magnetic. The conditions can then be reformulated in terms of the magnetic vector potential, A, merely by taking the dual[6,8], and this may be convenient for some purposes, particularly when combining the simplified model for some conductors with the conventional numerical description of others. The A network is shown diagrammatically in Fig. 6. The equations are obtained by inverting potential and flow quantities.

7. TEST EXAMPLE

The surface-node model has been tested in two dimensions by using it to compute the induced currents and losses in non-magnetic plates of various size subjected to a uniform applied field. This excitation demands a substantial amount of computing, because of the open boundary, but it removes what are otherwise arbitrary parameters from

the external field conditions. Results obtained by McWhirter and Thomas[9], and by Stoll[9], provide a convenient check, and these have been amplified by suitable numerical field solutions, using a sufficiently large number of nodes inside the conductor to give good accuracy. Two plate thicknesses, one equal to the skin depth, δ, as customarily defined, i.e.

$$t = \delta = d \sqrt{2}$$

and one of twice this value have been used for most of the calculations. These are sufficient to give large changes in the field quantities with depth, but the thickness is not so large as to prevent a significant interaction between the tangential fields penetrating from the two surfaces. In consequence the results are representative of the more critical range of parameters, well separated from the thin-plate model[5], at the one extreme, and the usual surface-element formulation at the other. In the surface-node model the h_x spacing between nodes was δ.

An important measure of accuracy is the behaviour of the normal component of the flux density, i.e. that penetrating through the plate. The magnitude and phase are plotted in Fig. 7, as a function of the distance in from the edge along the conductor centre-line, for a plate of half-width 8δ. The curves illustrate the close comparison between the results obtained by the two methods, and they also show the nature of the penetration in from the edge. The initial slopes of both the magnitude and phase curves are similar to those in plates of infinite thickness, but this small effective penetration depth is not representative of the plate as a whole.

The simplest, most sensitive and most useful single indication of accuracy is the total plate loss. This is plotted in Fig. 8 for a range of plate widths. As the width increases, so that the relative effect of the edges diminishes, the surface-node approximation gives results which agree to within about 1% with those obtained by the detailed, interior-node calculation. The error rises to 18% in a plate of half-width 3δ (that is, one which is modelled by only 4 nodes) but this may be reduced to 10% by halving the mesh interval.

The significance of the cross-plate (i.e. z-directed) branches in these calculations was investigated by repeating two calculations with them removed. This reduces the model to surface elements only, but allows for the interaction between the two surface layers. The plate half-width was again 8δ. In the plate of thickness δ the loss was found to be 0.033 of the correct value, this proportion rising to 0.15 in the plate of thickness 2δ. The unexpectedly low losses were accompanied by correspondingly low field components in quadrature time phase to the applied field. They show that, somewhat surprisingly, most of the current induced in plates of these sizes and proportions is due to the normal, not the tangential, component of the flux density - i.e. the dominant penetration mode is from the edge, not from the surfaces.

The internal node spacings chosen for the "exact" solution were

$$h_x = h_z = \delta/10,$$

so that 3381 interior and surface nodes would be needed to model a full plate of width 16δ and thickness 2δ, giving a similar accuracy as that obtained with only 34 surface nodes when the cross-plate branches were connected. The method thus gives considerable potential savings. Since rectangular meshes were used, the increased number of interior nodes in the "exact" calculation was also reflected in an increase in the number used in the exterior region. In testing the surface-node model the exterior node spacing h_z was the same as the plate thickness. The boundaries were sufficiently remote to have negligible effect.

8. CONCLUSIONS

It has been shown that models of flux screens and conducting plates in which the nodes are confined to the surfaces can give remarkably high accuracy provided that the usual surface-element approximation is suitably modified. Two modifications are necessary, one to allow for the interaction between the tangential fields penetrating from the two surfaces. But, more important, there is a second mode of penetration in from the edge which can be easily allowed for and which appears to have a dominant influence over a range of parameters of most interest in many practical applications. The modifications give a general form of surface-node model which can be applied to plates of any thickness having an adequate width/thickness ratio. It can be used for both two- and three-dimensional calculations, and provides a choice of potential function in two dimensions.

The method of analysis used gives a useful qualitative insight into the two modes by which flux penetrates into a plate and induces current, as well as a computer model by which the penetration can be predicted quantitatively. The accuracy of the model is being further investigated over a wide range of parameters, including thickness, mesh interval and permeability.

9. REFERENCES

1. Carpenter, C.J. and Wyatt, E.A. "Efficiency of numerical techniques for computing eddy currents in two and three dimensions", COMPUMAG, 1976, pp 242-250.
2. Carpenter, C.J. "Comparison of alternative formulations of 3-dimensional magnetic-field and eddy-current problems at power frequencies", Proc. I.E.E., 1977, 124, pp 1026-1034.
3. Carpenter, C.J. and Sharples, K.O. "Heating in transformer cores due to radial leakage flux. Pt. 2: Computed results", Proc. I.E.E., 1977, 124, pp 1181-1186.
4. Carpenter, C.J. "Theory of flux penetration into laminated iron, and associated losses", Proc. I.E.E., 1977, 124, pp 659-664.
5. Carpenter, C.J. and Djurovic, M. "Three-dimensional numerical solution of eddy currents in thin plates", Proc. I.E.E., 1975, 122, pp 681-688.
6. Carpenter, C.J. "A network approach to the numerical solution of eddy current problems", I.E.E.E. Trans. on Magnetics, 1975, MAG-11, pp 1517-1522.
7. Carpenter, C.J. "Finite element network models and their application to eddy-current problems", Proc. I.E.E., 1975, 122, pp 455-462.
8. Carpenter, C.J. "Magnetic equivalent circuits", Proc. I.E.E., 1968, 115, pp 1503-1511.
9. McWhirter, J.H. and Thomas, M.W. "Eddy-current losses in conducting slabs", Trans. I.E.E.E., 1971, PAS-90, pp 2373-2380.
10. Stoll, R.L. "Approximate formula for the eddy current loss in a long conductor of rectangular cross section by a transverse magnetic field", Proc. I.E.E., 1969, 116, pp 1003-1008.

10. APPENDIX - TANGENTIAL FIELD SOLUTION FOR A PLATE OF FINITE THICKNESS

The tangential field components in the plate can be calculated by the usual assumption that they vary only with z, giving solutions for both H_x and H_y of the form

$$H = K_1 \exp(\sqrt{j}\, z/d) + K_2 \exp(-\sqrt{j}\, z/d) \qquad (24)$$

Solving for the complex constants K_1 and K_2, and substituting in equations 14 and 15, gives similar expressions for Φ_x and Φ_y;

$$\Phi = (H_o + H_t)\mu_o \mu d\alpha \qquad (25)$$

where H_o and H_t are the appropriate tangential field values at the two surfaces, and α is given by equation 18. E_x and E_y vary in the same manner, so that the total current flowing in the plate is likewise given by

$$I = (E_o + E_t)\sigma d\alpha \qquad (26)$$

where, again, the suffices denote surface values. I, like Φ, has two components, defined by

$$I_x = \int_o^t J_x \, dz \qquad (27)$$

$$I_y = \int_o^t J_y \, dz \qquad (28)$$

and both are given by equation 26 in terms of the appropriate surface values.

Integrating Ampere's law (8) gives the surface H values in terms of the current,

$$H_{xt} - H_{xo} = I_y \qquad (29)$$

$$H_{yt} - H_{yo} = -I_x \qquad (30)$$

where the suffices x,y denote directions, and o,t the two surfaces. Likewise, from Faraday's law (5)

$$E_{xt} - E_{xo} = -j\omega \Phi_y \qquad (31)$$

$$E_{yt} - E_{yo} = j\omega \Phi_x \qquad (32)$$

and each Φ can accordingly be separated into two components, e.g.

$$E_{yo} = -j\omega \Phi_{xo} \qquad (33)$$

$$E_{yt} = j\omega \Phi_{xt} \qquad (34)$$

Eliminating between the equations in terms of these flux components, and the surface H values, gives equations 16 and 17.

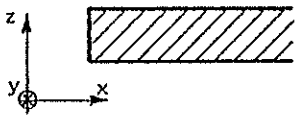

Fig.1 Conducting plate

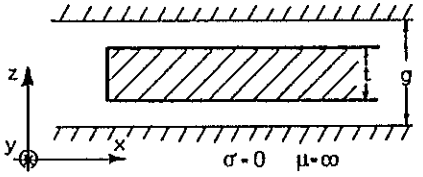

Fig.2 Plate in air gap

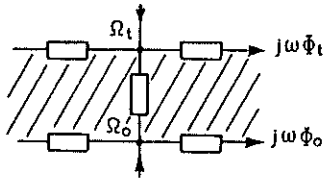

Fig.3 Network connections to surface node pair

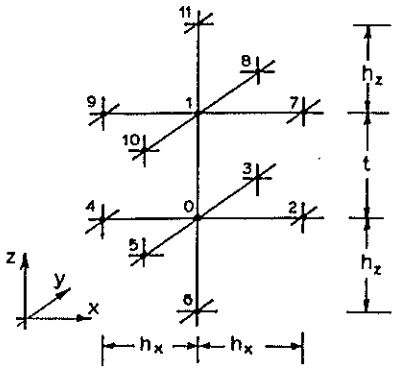

Fig.4 Node numbering convention

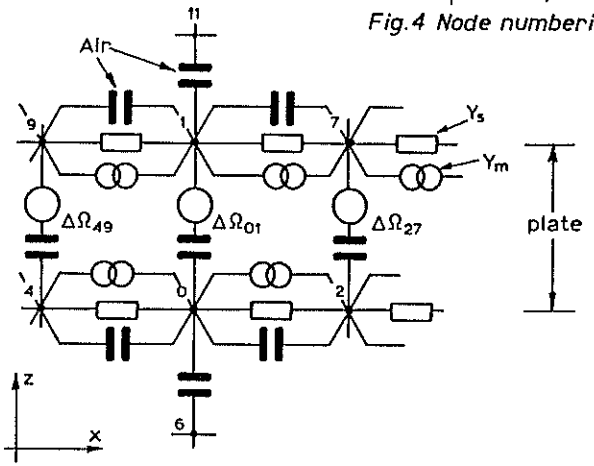

Fig.5 Equivalent magnetic network

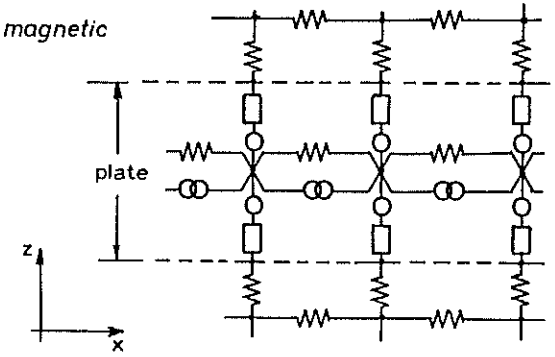

Fig.6 Two-dimensional magnetic vector potential (A) model

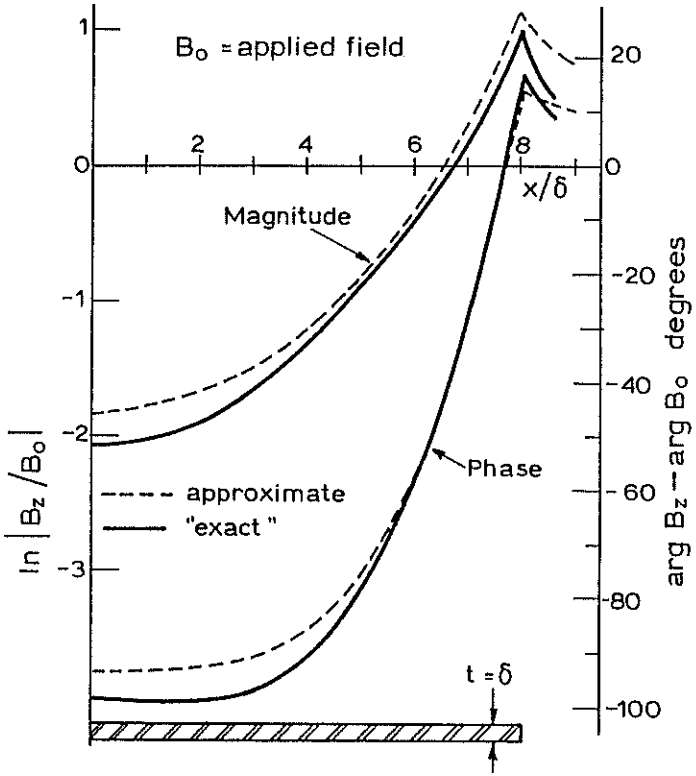

Fig.7 Penetration of B_z from edge

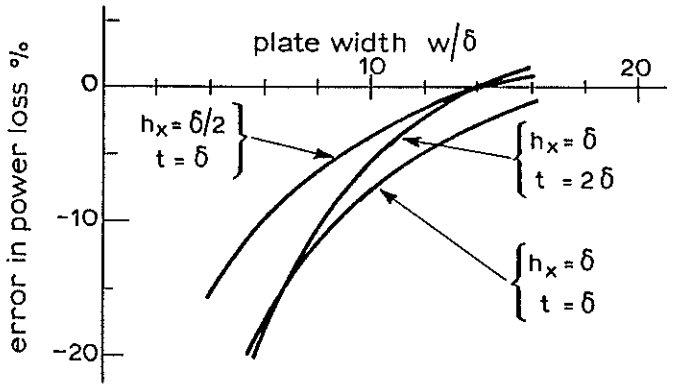

Fig.8 Error in total plate loss

FINITE ELEMENT MODELS OF EXTERIOR REGIONS CONTAINING MOVING CONDUCTORS.

D. A. Lowther* and P. P. Silvester+
*Imperial College, Dept. of Elect. Eng., London, SW7 2BT.
+McGill University, Elect. Eng. Dept., Montreal H3A 2A7, Canada.

ABSTRACT

An extension to the finite element technique is described which permits economic solution of open-boundary problems. The method can allow for both diffusive and moving media in the internal and exterior regions.

Results are given for a coil moving above a conducting plate which could be considered as a simulation of a levitated vehicle.

1. INTRODUCTION

Many practical electromagnetic induction problems involve both time-varying currents and moving media. Although in numerous cases two-dimensional modelling is appropriate, the media in question are often infinite in extent and thus require correspondingly infinite models. For example, a rectangular current-carrying coil moving parallel to an infinite, conductive half-space might be taken as a first electromagnetic model of a magnetically levitated vehicle. Here a major problem in numerical modelling arises from the eddy currents which, although locally dense, extend infinitely far in the half-space.

Classically, such problems have been treated by the introduction of artificial boundaries. In finite difference or finite element methods, it has been usual to model a large but finite section of the field, with arbitrarily imposed boundary conditions. On physical grounds, it has been argued that the nature of these conditions does not matter, provided they are imposed at a sufficiently distant boundary. Similarly, in approximate Fourier series solutions, arbitrary boundary conditions are imposed implicitly, by assuming periodicity, where none in fact exists.

Various attempts have been made in numerical modelling to create quasi-infinite finite difference meshes [1,2,3]. These reduce in essence to finding a discrete Green's function on an infinite, regular, finite difference mesh. Finding the continuum Green's function of the physical problem instead leads to a direct integral equation formulation, representing the local effect of infinitely remote boundaries [4,5,6].

In a recent paper [7] a recursive technique has been described by which a very large, topologically annular, Laplacian region can be given a very economic finite element representation. As in the earlier techniques, localised source distributions and fields can then be modelled by encasing a local ("interior") region of interest in a very large annular ("exterior") region. The interior region in this technique was allowed a broad variety of sources, material inhomogeneities, or nonlinearities. The exterior, however, was required to be purely Laplacian.

The present work extends the method described earlier, to allow diffusive and moving media in the exterior as well as interior regions. The relatively crude artificial boundaries found in earlier work [8,9] thus become unnecessary.

2. THEORY

2.1 The inclusion of the velocity term

If the finite element derivation is based on an energy balance then the inclusion of motion modifies the functional by adding a velocity dependent voltage. The basic diffusive field equation is:

$$\left(\left(\partial A/\partial x\right)^2 + \left(\partial A/\partial y\right)^2\right)/2\mu - JA = \sigma E A \qquad (1)$$

where E is a voltage given by

$$E = -\partial A/\partial t \qquad (2)$$

The corresponding element matrix E may be derived from the universal matrices given earlier [10] and, for a first order element, is given by:

$$E = \frac{\sigma\mu v}{6}\begin{bmatrix} b_1 & b_2 & b_3 \\ b_1 & b_2 & b_3 \\ b_1 & b_2 & b_3 \end{bmatrix} \qquad (3)$$

where V is a velocity in the x-direction.

The requirement of the problem functional to be rendered stationary may now be written as

$$(S + E)A = T.J$$

where S and T are matrices developed in previous work [11].

2.2 The exterior region problem

The basis of the method lies, as previously [7], in the ability to construct a series of annular regions around the solution area. These annuli have certain, well-defined, geometric properties:-

a) Each annulus is geometrically similar to every other annulus and all the annuli have the same internal finite element subdivision.

b) Each node on the inner boundary of an annulus is mapped onto a node on the outer boundary by a fixed mapping ratio with respect to a star point within the interior region (Figure 1).

c) The mapping ratio is the same for all annuli.

If the nodes on the first annulus are numbered so that all the inner perimeter nodes come first, the internal nodes next and the outer perimeter nodes last, then the S and E matrices for the annulus are given by:

$$\begin{bmatrix} S_{11} & S_{12} & S_{13} \\ S_{21} & S_{22} & S_{23} \\ S_{31} & S_{32} & S_{33} \end{bmatrix} \begin{bmatrix} \phi i \\ \phi c \\ \phi o \end{bmatrix} + \begin{bmatrix} E_{11} & E_{12} & E_{13} \\ E_{21} & E_{22} & E_{23} \\ E_{31} & E_{32} & E_{33} \end{bmatrix} \begin{bmatrix} \phi i \\ \phi c \\ \phi o \end{bmatrix} = 0 \quad (4)$$

The internal nodes may be removed by matrix condensation to give two new matrices in which the inner perimeter nodes are directly related to those on the outer perimenter:

$$\begin{bmatrix} S_{11} & S_{12} \\ S_{21} & S_{22} \end{bmatrix} \begin{bmatrix} \phi i \\ \phi o \end{bmatrix} + \begin{bmatrix} E_{11} & E_{12} \\ E_{21} & E_{22} \end{bmatrix} \begin{bmatrix} \phi i \\ \phi o \end{bmatrix} = 0 \quad (5)$$

The S and E matrices have been kept separate up to this point because they exhibit somewhat different properties.

The S matrix is symmetric and, in two-dimensional problems, its terms are independent of length. Hence each annulus has an identical S matrix and this fact can be used to accelerate the recursion process. In the Laplacian problem then, the maximal rate at which the outer boundary can be made to recede is given by

$$r^{2^k}$$

where r is the mapping ratio and k the number of recursion steps used.

The E matrix, however, is length dependent. The 'b' terms in equation 3 are functions of y. Consequently, although the E matrix has the same form for each annulus, the terms have to be multiplied by the mapping ratio applying to that annulus. The maximal rate at which the boundary recedes for the E matrix is then given by

$$r^k.$$

Unfortunately, for the moving conductor problem, the combined S and E matrices cannot be separated during the recursion process.

2.3 Finite thickness, infinitely long conductors

The description of the exterior region technique given above sets a restriction on the generation of the annuli. This is that the mapping procedure is related to a single star point within the interior space. This implies that the moving conductor becomes an infinite wedge (including the half-space as a special case). In most practical situations the conductor has a finite thickness and this requires a modification to the method of boundary generation.

In the problem of Figure 2, the single interior star point is replaced by two to allow for the infinite Laplacian half-spaces above and below the conductor. The conductor itself is extended using a one-dimensional mapping. This implies altering the S matrix as well as the E matrix at each boundary step. The procedure is relatively simple as the geometric dependence of each term of the S matrix is well defined.

3. EXAMPLES

The examples given in this section illustrate each of the stages outlined above for a simple coil moving above various conducting sheets. The data for each analysis was generated using the Mag-Net 78 system [12] allowing all the models to be produced and analysed in less than half a man-day.

3.1 Dual conductor problem - Laplacian

The first example shows a dual bus-bar problem with no ther conductors present and a simple Laplacian boundary. Figure 3 shows the flux plots obtained. The number of boundary steps, using the slow expansion, was 20 and the results agree with standard analytical results [13,14] to within 2%.

3.2 Dual coil, D.C. excitation, conducting half-plane

Figure 4 shows the same conductor geometry above a moving, conductive half-plane. The entry and exit effects can be seen in the figure. The presence of the exterior region is indicated by the way in which the flux lines 'cut' the boundary.

3.3 Dual coil, D.C. excitation, finite thickness plate

The conducting plate has now been given a finite thickness, otherwise conditions are the same as for section 3.2. Figure 5 shows the flux distribution with Figure 6 comparing calculated flux densities with those predicted by the theory of Freeman and Papageorgiou [15] one centimetre above the plate.

3.4 Dual coil A.C. excitation, finite thickness plate

The same model is considered as in section 3.3 but with 50 Hz a.c. excitation. Figures 7 and 8 show the instantaneous flux plots at times a quarter-cycle apart. It will be noted that both the spatial and temporal distributions are nonuniform, with the currents "sloshing" about in the solid conductor.

3.5 A more complex model

The model of Figure 9 shows a finite length iron block placed behind the coil above the conducting sheet. The coil is again a.c.

The flux plots, showing the effect of finite length stator iron, as in, for example, a short stator linear induction machine, are given in Figures 10 and 11.

As before, at least two plots are required to indicate how the spatial distribution of flux alters in time.

4. CONCLUSIONS

The exterior region approach earlier developed for Laplacian regions [7] has been extended to allow consideration of diffusive regions, such as might be found in problems involving eddy currents and/or motion. The technique is simple but has a slower convergence rate than the purely Laplacian problem. It is also interesting to note that, unlike the Laplacian problem, the E_{12} and E_{21} terms do not approach

zero as the boundary recedes. The reason is that the coupling terms give a measure of the current present in the exterior region. Consequently the inner and outer boundaries are not de-coupled in the same way as in the Laplacian solution.

The method lends itself to automatic exterior mesh generation and the entire region can be computed from a knowledge of the node positions on the inner boundary. Consequently the boundary condition can be applied without user interaction.

The technique is also computationally fast; typically taking around 10% of the solution time for a complete problem to generate and condense the exterior region. Because the number of inner boundary nodes is relatively few (for a uniform rectangular mesh the ratio of total to boundary nodes being around $\pi/4$) the sparsity of the complete S matrix is only slightly affected.

The theory described here has considered only velocities in the x direction, similarly velocities in the y direction or rotational velocities can be included 17. The method can be used to analyse the general 2-D problem of a coil moving in an arbitrary direction relative to an arbitrary number of conducting bodies. Hence, on a step by step basis, the complete dynamic behaviour of a propulsion system together with its suspension can now be examined.

5. REFERENCES

1. Cermak, I A and Silvester, P: Solution of Two-dimensional Field Problems by Boundary Relaxation, Proc. IEE, 115, 1341-1348, 1968.
2. Sandy, F and Sage, J: Use of Finite Difference Approximations to Partial Differential Equations for Problems Having Boundaries at Infinity, IEEE-MTT19, 484-486, 1971.
3. Amstutz, P: Sur la Solution Élementaire d'une Équation de Laplace Concrétisée, Annales des Télécommunications, 22, 149-152, 1967.
4. Silvester, P and Hsieh, M-S: Finite-element Solution of 2-Dimensional Exterior-Field Problems, B Proc. IEE, 118, 1743-1747, 1971.
5. McDonald, B H, Friedman, M and Wexler, A: Variational Solution of Integral Equations, IEEE-MTT22, 237-248, 1974.
6. Zienkiewicz, O C, Kelly D W and Bettess, P: The Coupling of the Finite Element Method and Boundary Solution Procedures, Int. J. Numer. Methods Eng., 11, 355-375, 1977.
7. Silvester, P P, Lowther, D A, Carpenter, C J and Wyatt, E A: Exterior Finite Elements for 2-Dimensional Field Problems with Open Boundaries, Proc. IEE, 124, 1267-1270, 1977.
8. Foggia, A, Sabonnadiere, J C and Silvester, P: Finite Element Solution of Saturated Travelling Magnetic Field Problems, IEEE-PAS94, 866-871, 1975.
9. Ja'far Al-Rikabi: M.Sc. Thesis: Baghdad, 1976.
10. Silvester, P: Construction of Triangular Finite Element Universal Matrices, Int. J. Numer. Methods Eng., 12, 237-244, 1978.
11. Silvester, P: High-order Polynomial Triangular Finite Elements for Potential Problems, Int. J. Engng. Sci., 7, 849-861, 1969.
12. Silvester, P P: The Mag-Net 78 Finite Element Problem Description Language, Proc. US-Japan Interdisciplinary Symposium on Finite Elements, 1978 (in press).
13. Strutt, M J O: Das Magnetische Feld Eines Rechteckigen von Gleichstrom Durchflossenen Leiters, Arch. Eltrotech., 17, 533-535, 1927.
14. Binns, K and Lawrenson, P J: Analysis and Computation of Electric and Magnetic Field Problems, Pergamon, 1963.
15. Freeman, E M and Papageorgiou, C P: Spatial Fourier Transforms - A New View of End Effects in Linear Induction Motors, Proc. IEE, 125, 747-753, 1978.
16. Lowther, D A, Rajanathan, C B and Silvester, P P: A Finite Element Technique for Solving 2-D Open Boundary Problems, IEEE-Mag., to be published.
17. Hwang, J H and Lord, W: Finite Element Analysis of the Magnetic Field Distribution Inside a Rotating Ferromagnetic Bar, IEEE-Mag10, 1113-1118, 1974.

ACKNOWLEDGEMENTS

The work described in this paper resulted from visits sponsored by the U. K. Science Research Council. The authors would like gratefully to acknowledge the financial support of the U. K. Science Research Council and of the National Research Council of Canada.

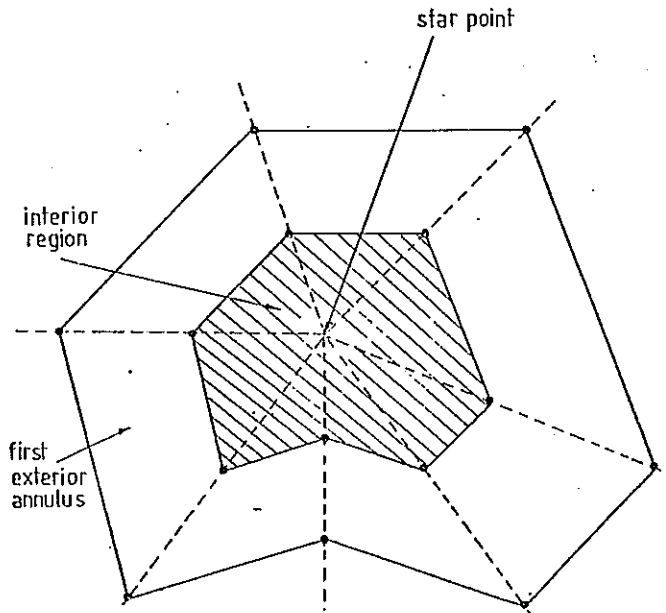

Figure 1 Basic exterior annulus

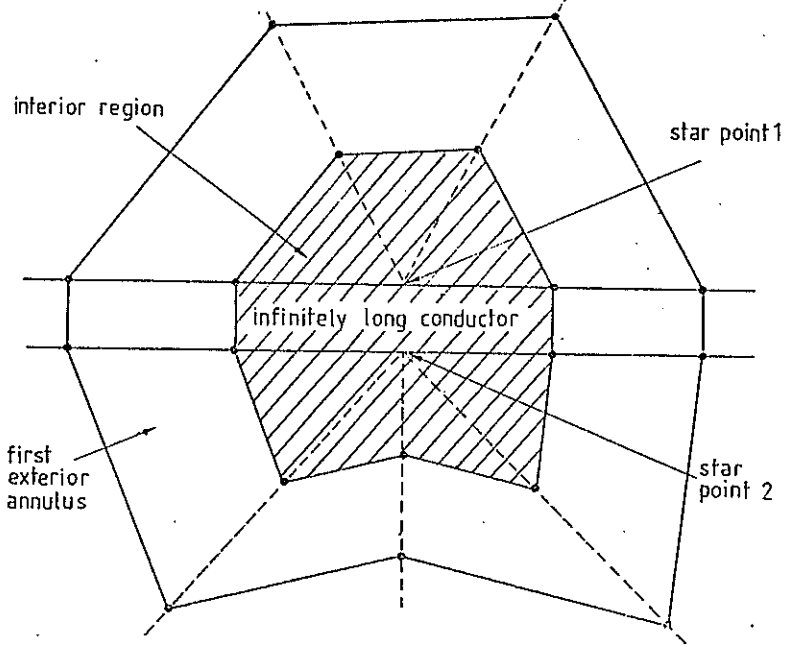

Figure 2 Modification for finite thickness conductor

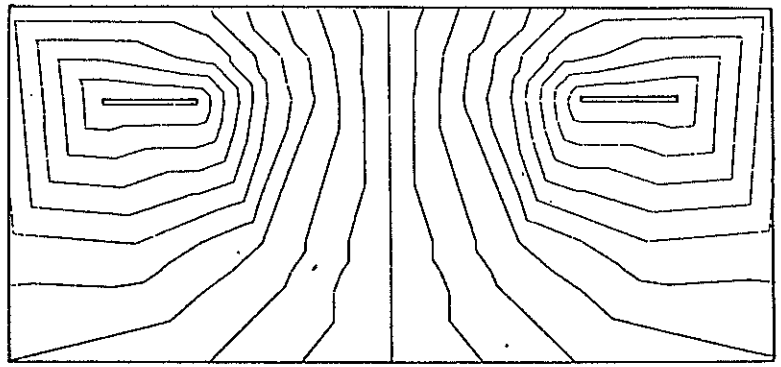

Figure 3 Stationary D.C. Coil in air

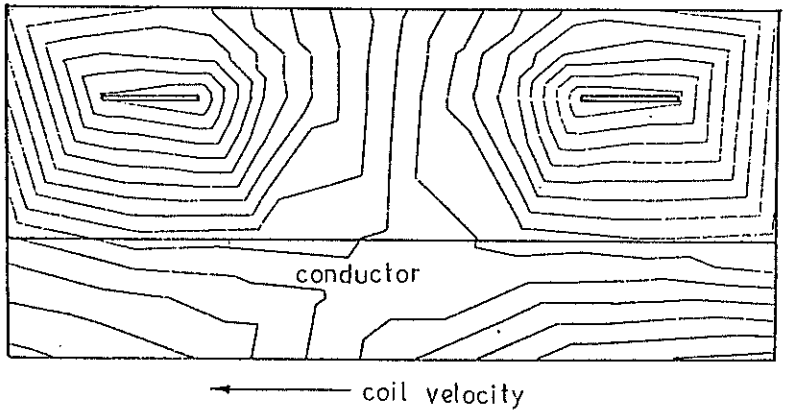

Figure 4 Moving D.C. Coil above infinite conductor

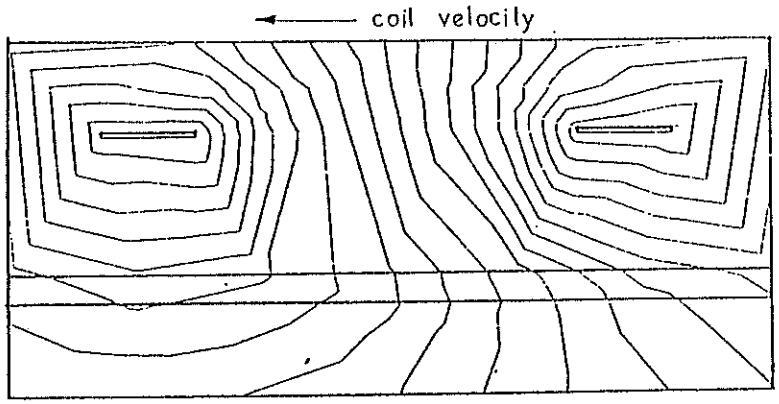

Figure 5 D.C. Coil moving above finite thickness plate

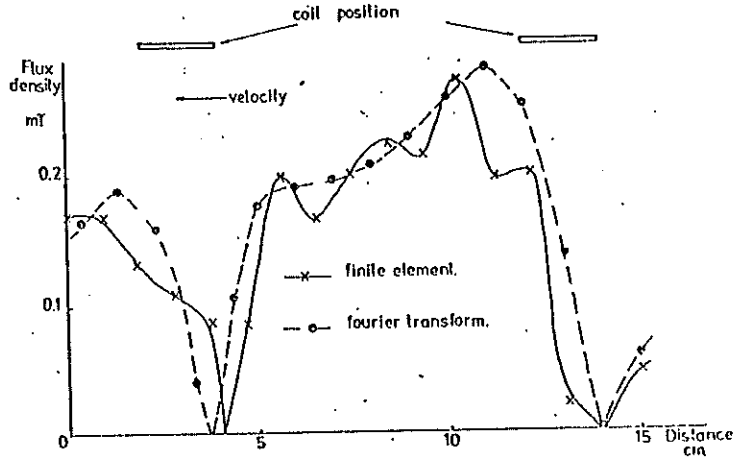

Figure 6 Calculated flux density for figure 5

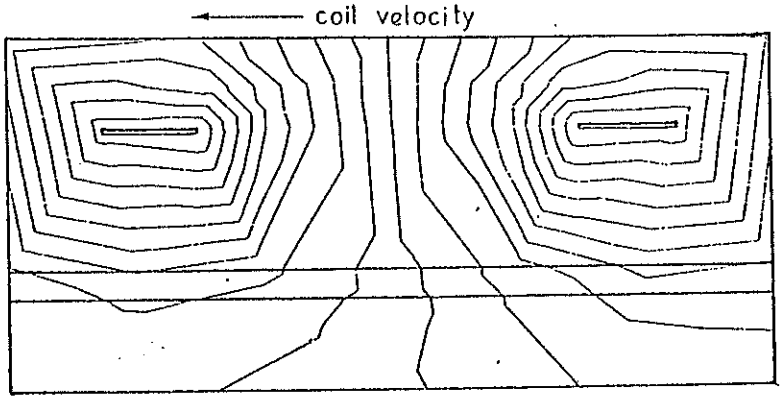

Figure 7 Moving A.C. Coil, in phase field component

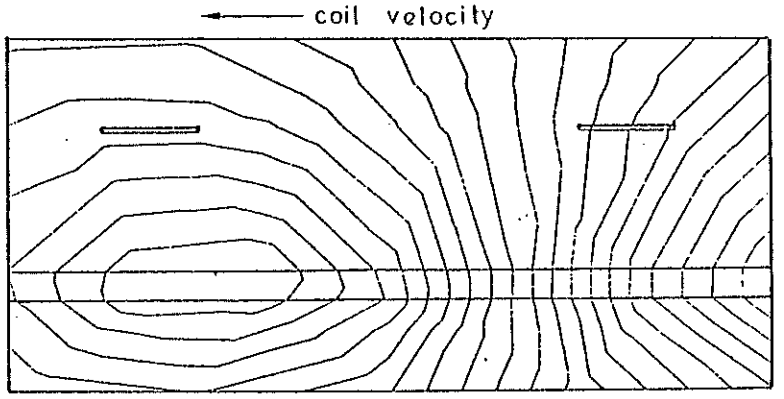

Figure 8 Moving A.C. Coil, quadrature phase component

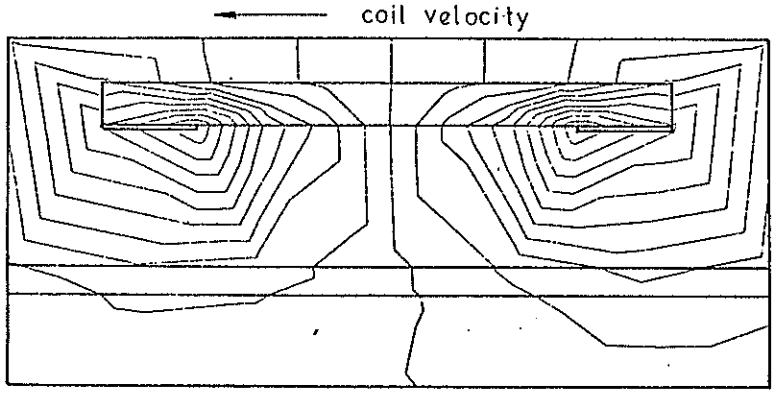

Figure 9 Moving iron/coil combination, in phase field component

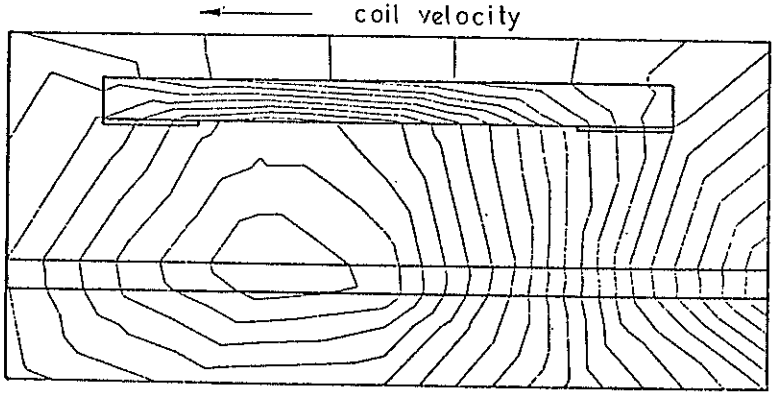

Figure 10 Moving iron/coil combination, quadrature field component

DEVELOPMENTS IN THE RUTHERFORD LABORATORY EDDY CURRENT PROGRAM

C S Biddlecombe
Rutherford Laboratory, Chilton, Didcot, Oxon, OX11 0QX

ABSTRACT

Further developments to the Integral Equation Method for eddy currents are described. These are a new method for time stepping, the treatment of asymmetry, and the inclusion of permeable material. Results are compared with analytical methods and measurements.

1. INTRODUCTION

This paper restates the algorithm for the solution of eddy current problems by an integral equation method, and details the developments made since its first publication.[1] These are the inclusion of permeable material, a new time stepping procedure, and the treatment of asymmetric geometries.

The two-dimensional limit of one component of current density and two of magnetic field is treated, although the method is applicable to the other limit, and can in theory, be extended to three dimensions.

The eddy current and permeable regions are represented by infinite prisms, over which current density and magnetisations are assumed to be uniform. The current densities are connected by an integral equation in terms of magnetic vector potential, and the magnetisations in terms of magnetic field strength.

A new, and as yet untested method, using the magnetic vector potential throughout, is suggested to improve the solution of the permeable regions.

2. THE INTEGRAL EQUATIONS

The integral equation method is based on the assertion that the field quantities at a point can be expressed as a sum of contributions from all sources. Thus, using subscripts J, M and D to denote eddy currents, magnetisations and driving fields, the magnetic vector potential:

$$A = A_J + A_M + A_D \tag{2.1}$$

and the magnetic field strength:

$$H = H_J + H_M + H_D \tag{2.2}$$

Analytic expressions exist for A_J, A_M, H_J and H_M:

$$A_J(\underline{r}) = \frac{\mu_o}{4\pi} \int \frac{J(\underline{r}')}{|\underline{r} - \underline{r}'|}\, dv' \tag{2.3}$$

$$A_M(\underline{r}) = \frac{\mu_o}{4\pi} \int M(\underline{r}'') \times \nabla \left(\frac{1}{|\underline{r} - \underline{r}''|}\right) dv'' \tag{2.4}$$

$$H_J(\underline{r}) = \int J(\underline{r}') \times \frac{(\underline{r} - \underline{r}')}{4\pi|\underline{r} - \underline{r}'|^3}\, dv' \tag{2.5}$$

$$H_M(\underline{r}) = -\nabla \int M(\underline{r}'').\nabla\left(\frac{1}{4\pi|\underline{r}-\underline{r}''|}\right)dv'' \tag{2.6}$$

A_D and H_D are known. Thus the total field can be expressed in terms of the unknown current density and magnetisation source strengths, with the driving field.

The current density can be eliminated using Maxwell's second equation:

$$\nabla \times E = \frac{-\partial B}{\partial t} \tag{2.7}$$

the definition of magnetic vector potential:

$$\nabla \times A = B \tag{2.8}$$

and Ohm's Law:

$$J = \sigma E \tag{2.9}$$

Substituting (2.8) into (2.7):

$$\nabla \times E = -\frac{\partial}{\partial t}(\nabla \times A) \tag{2.10}$$

and integrating:

$$E = -\left(\frac{\partial A}{\partial t} + \nabla\phi\right) \tag{2.11}$$

Using (2.9):

$$J = -\sigma\left(\frac{\partial A}{\partial t} + \nabla\phi\right) \tag{2.12}$$

where ϕ is a scalar potential. In the limit considered by this paper, the potential can be, in most cases, ignored, since there are no surfaces perpendicular to the current. It is useful, as will be shown in treating eg. the mid-plane of a asymmetric three-dimensional object.

The total field strength can also be eliminated, if the field point is within the permeable material:

$$H = \frac{M}{X} \tag{2.13}$$

3. DISCRETISATION

Only the eddy current and permeable regions need discretisation, and, using zero order elements, (2.3-6) become integrals over the cross-sections of infinite prisms. They are evaluated by the method suggested by Collie.[2]

The field points are chosen to be the centroids of the elements. Thus equation (2.1) becomes:

$$A_i = A_{Di} + \sum_{j=1}^{c} R_{ij} \left(\frac{\partial A}{\partial t}\right)_j + \sum_{\ell=1}^{p} \left[S_{i,2\ell-1} M_{x\ell} + S_{i,2\ell} M_{y\ell} \right] \qquad (3.1)$$

for $i = 1,2,3....c$

and (2.2) becomes:

$$0 = H_{Dxk} + \sum_{j=1}^{c} T_{2k-1,j} \left(\frac{\partial A}{\partial t}\right)_j + \sum_{\ell=1}^{p} \left[\left(U_{2k-1,2\ell-1} - \frac{\delta_{k\ell}}{X}\right) M_{x\ell} + U_{2k-1,2\ell} M_{y\ell} \right] \qquad (3.2)$$

and

$$0 = H_{Dyk} + \sum_{j=1}^{c} T_{2k,j} \left(\frac{\partial A}{\partial t}\right)_j + \sum_{\ell=1}^{p} \left[U_{2k,\,2\ell-1} M_{x\ell} + \left(U_{2k,2\ell} - \frac{\delta_{k\ell}}{X}\right) M_{y\ell} \right] \qquad (3.3)$$

for k = 1, 2, 3 ...p, where c is the number of eddy current elements and p, the number of permeable elements. The coefficients R,S,T,U and the integrals in (2.3-6) with the appropriate signs and constants.

A matrix of equations can now be formed, sub-matrix G_A formed from coefficients R, G_B from S, G_C from T and G_D from U and U-δ.

$$\begin{bmatrix} A - A_D \\ \hline - H_D \end{bmatrix} = \begin{bmatrix} G_A & G_B \\ \hline G_C & G_D \end{bmatrix} \begin{bmatrix} \partial A/\partial t \\ \hline M \end{bmatrix} \qquad (3.4)$$

4. SOLUTION OF EQUATIONS

The equations (3.4) could be solved as they stand. The method chosen, however, involves a modification of the matrix G_D, and a reduction in the number of equations first.

Defining H_j as the total field from all currents, the second line of equation (3.4) can be written:

$$G_D M = - H_j \qquad (4.1)$$

This could be solved directly for M. However the matrix Gd is severly ill-conditioned, especially if the permeability is high. In such cases direct solution leads to looping in the magnetisation vectors [3], although the field values outside the iron are virtually unaffected. This can be cured by several methods.[4] The method chosen is regularisation since it involves only one change to the matrix and no iterative procedures, which would be needed at each time step. Equation (4.1) is substituted with the minimisation of:

$$||G_D M + H_j||^2 + \alpha||M||^2 \qquad (4.2)$$

with respect to M. This leads to the equation:

$$M = (G_D^T G_D + \alpha I)^{-1} G_D^T H_j \qquad (4.3)$$

which can be written exactly as equation (4.1) after the necessary transformation of matrix G_D.

A small value of α is chosen which removes the looping, but does not affect the values of field outside the permeable material.

$$\alpha = 4 \times 10^{-5} \max_{i,j} (G_{Dij})^2 \qquad (4.4)$$

To reduce the number of equations, the second line of equation (3.4) can be written:

$$G_C \frac{dA}{dt} + G_D M = - H_D \qquad (4.5)$$

Rearranging:

$$M = - G_D^{-1} \left(H_D + G_D \frac{dA}{dt}\right) \qquad (4.6)$$

Substituting into the top line of equation (3.4):

$$\left[G_A - G_B G_D^{-1} G_C\right] \frac{dA}{dt} = A - A_D + G_B G_D^{-1} H_D \qquad (4.7)$$

The matrix of coefficients is now (c x c) and $A_o = A_D - \left[G_B G_D^{-1} H_D\right]$ is the combined driving field. Equation (4.7) can therefore be written more clearly:

$$G \frac{dA}{dt} = A - A_o \qquad (4.8)$$

The solution could have been further simplified by limiting the problems solvable to steady state sinusoidal excitations and treating real and imaginary parts separately. However it was decided to solve equations as an initial-value problem (4.8) for transient eddy currents.

Three methods are used; a fourth order Runge-Kutta method, an eigenvalue method and Gear's method. The last two are described here:

4.1 Eigenvalue Method

The eigenvalue method depends on the eigenvalues of the inverse G matrix being distinct. This property enables a similarity transformation to diagonal form:

$$P^{-1}\, G^{-1}\, P = D \tag{4.9}$$

where D is a diagonal matrix, the diagonal members being the eigenvalues, and the matrices P and P^{-1} contain the right and left eigenvectors. Thus equation(4.8) can be written:

$$\frac{dA}{dt} = P\, D\, P^{-1}\, (A - A_o) \tag{4.10}$$

Pre-multiplying by P^{-1} and rearranging:

$$\frac{d}{dt}\,(P^{-1}\, A) - (D\, P^{-1}\, A) = -\,(D\, P^{-1}\, A_o) \tag{4.11}$$

Putting $y = P^{-1}\, A$, the equations can be separated:

$$(\frac{d}{dt} - D_i)\, y_i = -\,(D\, P^{-1}\, A_o)_i \tag{4.12}$$

This can be integrated multiplying both sides by

$$e^{-D_i t}$$

$$y_i e^{-D_i t} = \int_o^t e^{-D_i t}\, (D\, P^{-1}\, A_o)_i\, dt \tag{4.13}$$

Providing such an integral exists A is readily obtainable

$$A = P\, y \tag{4.14}$$

$\frac{dA}{dt}$, J and M can be found from equations (4.8),(2.12) and (4.6).

The main advantage of the eigenvalue method is its speed, being unaffected by changes in time constants caused by varying geometry or element parameters. Results can be calculated for any value of time without integrating numerically through previous times.

4.2 Gear's Method

Gear's method is a predictor-corrector type method modified to solve stiff systems of ordinary differential equations.[5] Stiff systems are those with a large ratio of the largest to smallest eigenvalues of the matrix $[d^2A/dt.dA]$. Such cases occur frequently, especially with unconnected conductor regions (see section 5 below).

Gear's method is reserved for cases which have repeated eigenvalues.

5. CONNECTIVITY

Connectivity is the name given to the "end" properties of the conductors. Connected conductors have a return path for current defined by symmetry. Unconnected conductors do not, and for them the conservation of charge must be applied, ie:

$$\int J\, ds = 0 \tag{5.1}$$

In other words, there must be no net current flow. Although this cannot be applied in a strictly infinite problem its application makes the two dimensional limit useful in solving real problems, where the condition does apply.

This is where the scalar potential, equation (2.11) matters. Equation (4.8) should in these cases be written:

$$G\,(\frac{dA}{dt} + \text{grad}\ \phi) = A - A_o \tag{5.2}$$

although this equation can be derived exactly as before. The grad term can be eliminated by introducing a new vector potential, A'.

$$\frac{dA'}{dt} = \frac{dA}{dt} + \text{grad}\ \phi \tag{5.3}$$

Then by integrating:

$$A' = A + f(t) \tag{5.4}$$

Thus equation (5.2) becomes:

$$G\,\frac{dA'}{dt} = (A' - A_o - f(t)) \tag{5.5}$$

Equation (5.1) can be discretised:

$$\sum_{i=1}^{nc} \frac{dA'}{dt_i}\, \sigma_i\, a_i = 0 \tag{5.6}$$

where σ_i and a_i are the conductivity and area of element i, and the elements i are all part of one unconnected region. Equation (5.6) is equivalent to:

$$\sum_i \sigma_i a_i \left[\sum_{j=1}^{nc} (G^{-1})_{ij} \left[(A' - A_o)_j - f(t)_j \right] \right] = 0 \qquad (5.7)$$

for all elements i in any one region. By defining matrices R, S and T:

$$R_{k\ell} = \sum_i \sum_j (G^{-1})_{ij} a_i \sigma_i \qquad (5.8)$$

i ε region k

j ε region ℓ

$$S_{kj} = \sum_i (G^{-1})_{ij} a_i \sigma_i \qquad (5.9)$$

i ε region k

$$T_{ik} = \sum_j (G^{-1})_{ij} \qquad (5.10)$$

j ε region k

and noting that f(t) is constant over each region

$$f(t) = R^{-1} S(A - A_o) \qquad (5.11)$$

Since f(t) is in terms of $(A-A_o)$ a new matrix can be formed:

$$G^{-1}_{new} = G^{-1}_{old} - \left[T R^{-1} S \right] \qquad (5.12)$$

Solution proceeds as in other cases, but net current is ensured zero in each region. Since one zero eigenvalue is found for each unconnected region the eigenvalue method might fail with two or more such regions.

The above method has been tested by comparing the currents induced by a uniform external field, in a symmetric bar, represented by symmetry, with those in a completely specified bar, of the same overall dimensions. Without the connectivity condition, the results only coincide when the bar is placed symmetrically about the zero of magnetic vector potential. With the condition, agreement can be obtained at all levels of potential.

6. RESULTS

Results from a program, BUEDDY, written by the author, have been compared with analtyical solutions and measurements. The analytical test case is the hollow cylinder, inside radius 0.1m and outside radius 0.2m. It is made of either copper, with conductivity $10^8 Sm^{-1}$, or iron, with conductivity $10^6 Sm^{-1}$ and relative permeability 1000. The driving field is of 1 T perpendicular to the axis of the cylinder. It is switched on at zero time and the transient response is calculated.

The results tabulated (Table 6.1) are of induced flux density, in line with the applied field, at radial positions, also in line with the field.

Table 6.1 Results of Cylinder test

	position [m]	Induced Flux Density B_y [T]			
		Numbers of Elements			Analytic
		20	40	60	
Cu Time = 0.0025	0.0	-1.000	-1.000	-1.000	-1.000
	0.1	-1.000	-1.000	-1.000	-1.000
	0.2	-0.943	-0.941	-0.964	-0.950
	0.3	-0.393	-0.405	-0.416	-0.423
Cu Time = 0.5	0.0	-0.645	-0.652	-0.654	-0.658
	0.1	-0.650	-0.654	-0.655	-0.658
	0.2	-0.385	-0.389	-0.389	-0.391
	0.3	-0.167	-0.171	-0.172	-0.164
		30	42	56	
Fe Time = 0.0125	0.005	-1.017	-1.014	-1.011	-1.000
	0.105	-1.013	-1.015	-1.018	-1.000
	0.205	1.323	1.212	1.124	0.885
	0.305	0.358	0.359	0.359	0.400
Fe Time = 2.5	0.005	-0.968	-0.975	-0.980	-0.996
	0.105	-1.213	-1.152	-1.106	-0.816
	0.205	1.123	1.074	1.040	0.947
	0.305	0.419	0.442	0.423	0.428

Convergence towards the analytical solution is obvious in the case of copper. The iron results are less pleasing, but are still within the right order of magnitude.

Figures 6.1-4 show flux lines and discretisations. Except for the 60 element, copper case the discretisations do not make use of any prior knowledge of skin effect.

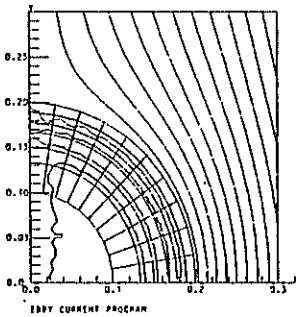

Fig 6.1 Copper cylinder,
60 elements
time = 0.0025s

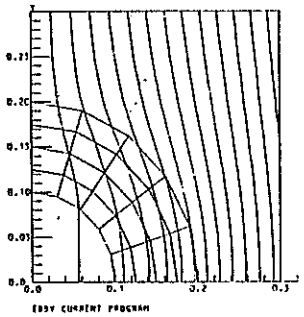

Fig 6.2 Copper cylinder,
20 elements
time = 0.5s

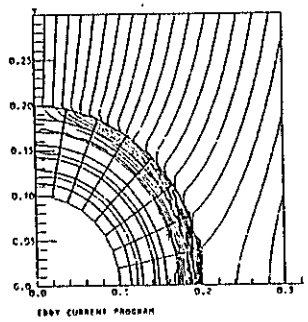

Fig 6.3 Iron cylinder,
56 elements
time = 0.0125s

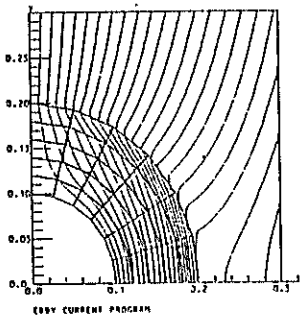

Fig 6.4 Iron cylinder,
30 elements
time = 2.5s

For comparison with measurements, a linear induction motor, made and tested at Imperial College, was used. For this the RMS flux density in the airgap, and force on the plate as the plate is displaced, are shown graphically in figures 6.5-8. The computer model is shown in figure 6.9, the broken lines indicating that part of the model treated by symmetry.

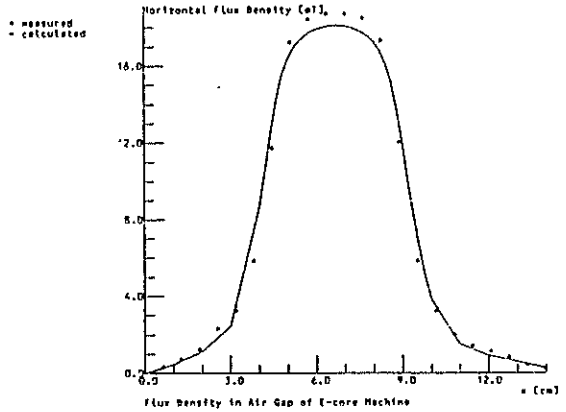

Fig 6.5 RMS Horizontal flux in gap of E-core machine

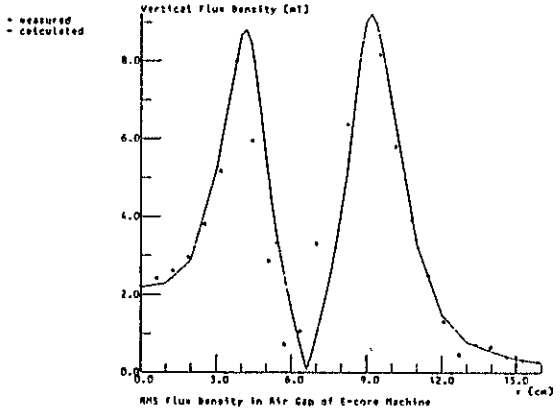

Fig 6.6 RMS Vertical flux in gap of E-core machine

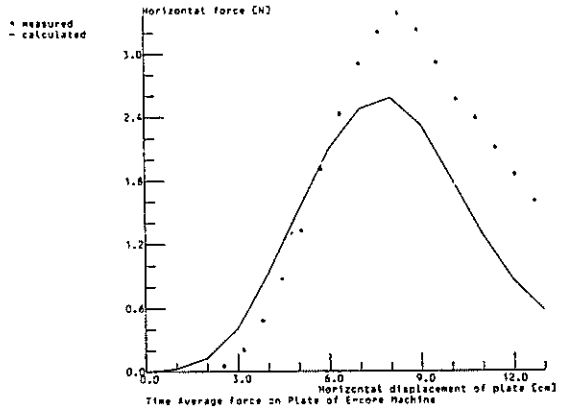

Fig 6.7 Horizontal force on plate of E-core machine

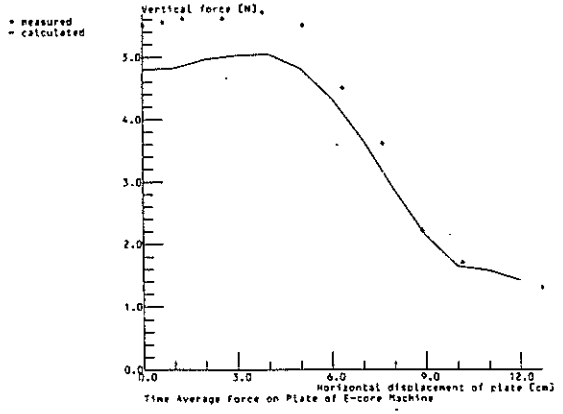

Fig 6.8 Vertical force on plate of E-core machine

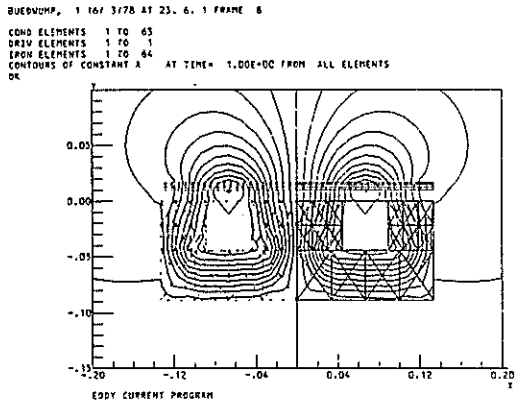

Fig 6.9 Element structure and flux lines of E-core machine

The poorer results for forces are attributed to two factors. Since the force was calculated at different horizontal positions of the plate, symmetry could not be employed. The same number of elements was used, covering the whole model, thus giving a coarser discretisation. Also, the force is a second order effect, depending on current density and flux density values.

7. ALTERNATIVE TREATMENT FOR IRON

To improve the results for iron, especially conducting iron, an alternative formulation is proposed. It starts from the expression for magnetic vector potential due to a magnetisation source (2.4):

$$A_M(\underline{r}) = \frac{\mu_o}{4\pi} \int M(\underline{r}'') \times \nabla\left(\frac{1}{|\underline{r} - \underline{r}''|}\right) dv \qquad (7.1)$$

The magnetisation can be expressed in terms of the field strength (2.13)

$$M = \chi H \qquad (7.2)$$

which can, in turn, be expressed in terms of the vector potential

$$H = \frac{1}{\mu} \nabla \times A \qquad (7.3)$$

Therefore

$$A_M(\underline{r}) = \frac{\mu_o}{4\pi} \int \frac{\chi}{\mu} \nabla \times A \times \nabla\left(\frac{1}{|\underline{r} - \underline{r}''|}\right) dv'' \qquad (7.4)$$

In two dimensions, A has only a Z component. Therefore (7.4) can be simplified, using the two dimensional form of (7.1)

$$A_M(\underline{r}) = -\frac{\mu_o}{2\pi} \int \frac{M(\underline{r}'') \times (\underline{r} - \underline{r}'')}{|\underline{r} - \underline{r}''|^2} da \qquad 7.5$$

to the following form

$$A_M(\underline{r}) = -\frac{\mu_o}{2\pi} \int \frac{\chi}{\mu} \nabla A(\underline{r}'') \cdot \nabla(\log(\underline{r} - \underline{r}''))da \qquad (7.6)$$

This can be transformed using Green's theorem[6] to a boundary term and a volume term.

$$A_M(\underline{r}) = -\frac{\mu_o}{2\pi} \int \frac{\chi}{\mu} A(\underline{r}'') \frac{d}{dh} \log(\underline{r} - \underline{r}'') ds + \frac{\mu_o}{2\pi} \int A(\underline{r}'') \nabla \cdot \left(\frac{\chi}{\mu} \nabla (\log(\underline{r} - \underline{r}''))\right) da \qquad (7.7)$$

For linear problems, this can be further simplified, since the second term is zero except at the field point.

The final form for the total vector potential is

$$A(\underline{r})\left(1 - \mu_o \frac{\chi(\underline{r})}{\mu(\underline{r})}\right) = A_D(\underline{r}) + \frac{\mu_o}{2\pi} \sigma(\underline{r}') \int \frac{\partial A}{\partial t}(\underline{r}') \log(\underline{r} - \underline{r}') dx\, dy - \frac{\mu_o}{2\pi} \int \frac{\chi(\underline{r}'')}{\mu(\underline{r}'')} A(\underline{r}'') \frac{d}{dn} (\log(\underline{r} - \underline{r}''))' ds \qquad (7.8)$$

Permeable regions can now be treated by discretising only the boundary. The integral equation in terms of field strength can be replaced by a second equation in terms of vector potential, the field points being the boundary nodes. This method derives from the work on 3D magnetostatics at the Rutherford Laboratory.[7]

8. CONCLUSIONS AND FUTURE WORK

As it stands, the integral equation method is a powerful way in which to solve eddy current problems in two dimensions. If the modifications suggested in section 7 give the hoped for improvements, it will be worth extending to a steady state version, and investigating extensions to the eigenvalue method, for repeated eigenvalues. Other applications could be axisymmetry and moving conductors.

9. ACKNOWLEDGEMENTS

The author would like to thank his colleagues at the Rutherford Laboratory for their help in this work, especially Mr C.W. Trowbridge and Mr J Simkin for their technical advice and Mrs P. Morgan for her preparation of the typescript.

10. REFERENCES

1. Biddlecombe, C S, Collie, C J, Simkin, J and Trowbridge, C W. The Integral Equation Method Applied to Eddy Currents. Proc COMPUMAG Conference on the Computation of Magnetic Fields, Oxford, 1976.

2. Collie, C J. Magnetic Fields and Potentials of Linear Varying Current or Magnetisation in a Plane Bounded Region. Proc COMPUMAG Conference on the Computation of Magnetic Fields, Oxford, 1976.

3. Aleshaev, A N, Dzjuba, V A, Karlinger, M M, Lisjynski and Fomel, P M. Correction of the Direct Method of Calculation of Static Magnetic Fields in Systems with Iron, Preprint IYF 75-95, Institut Yadernoi Fizike, Soan, USSR.

4. Miller, G F. Fredholm Equations of the First Kind, Ch.13 of Numerical Solution of Integral Equations, edited by Delves, L M and Walsh, J, Clarendon Press, Oxford, 1974.

5. Craigie, J A I. A Variable Order Multistep Method for the Numerical Solution of Stiff Systems of Ordinary Differential Equations. Numerical Analysis Report 11, University of Manchester, 1975.

6. Smythe, W R. Static and Dynamic Electricity, ch 3, McGraw-Hill, London, 1968.

7. Armstrong, A G A M, et al. Proc. COMPUMAG Conference on the Computation of Magnetic Fields, Grenoble, 1978.

THE EFFECT OF GAPS BETWEEN LAMINATIONS ON AXIAL FLUX AND EDDY CURRENTS IN AN IDEALISED STATOR CORE

T.G. Phemister and C. Wymer

N.E.I. Parsons Ltd., Newcastle upon Tyne, NE6 2YL, England

ABSTRACT

The effect of gaps between laminations on axial flux and eddy currents has been calculated for an idealised model of a stator core which corresponds roughly to what happens in an actual generator more than 100 mm from the core end. Equations have been formulated and solved for half-lapped and third-lapped cores. Compared with calculations for a core without gaps, for the same axial flux density at the inner and outer surfaces, the gaps increase the total axial flux by about a fifth and the total eddy current loss by about a third.

1. INTRODUCTION

Calculations of the three-dimensional magnetic field in a generator stator core necessarily use a smoothed or homogeneous[1] representation of the laminated structure. The number of layers of laminations in the first half metre of the core is of order a thousand and no computation could contain so much detail. Nevertheless, the presence of electrical discontinuities in the core and the fact that they are staggered in neighbouring layers must have a significant effect on the axial component of flux density. It is this effect which has been investigated for an idealised stator core.

The model adopted is a stack of rectangular laminations of finite width in the direction corresponding to radial in an actual machine, but extending to infinity in the other two directions. Thus there are no end effects and every lamination has the same pattern of electromagnetic fields, though the pattern is staggered in adjacent layers. The permeability of the iron is assumed to be linear, but this is of no importance because the pattern of the fields is determined by a skin-depth almost entirely dependent on the stacking factor. The model corresponds roughly to what happens in an actual generator stator core more than 100 mm from the end.

A companion paper[2] generalises the equations so that the effect of the gaps on fields near the core end can be investigated.

2. TYPES OF LAPPING CONSIDERED

Two types of lapping are considered: half lapping (Fig. 1a), in which the gaps between laminations in one layer are opposite the middle of the laminations in the neighbouring layer; and third lapping (Fig. 1b), in which the gaps in the neighbouring layer are displaced by one third of the width of the lamination.

The same coordinate system is used for both lappings. The x-axis corresponds to the circumferential direction in an actual stator, and the y-axis to the radial direction (Fig. 2). The boundaries $y = \pm w$ are the finite boundaries of the infinite stack of laminations and correspond, respectively, to the outer radius and the radius of the bottom of the slots in an actual stator. The other boundaries of the lamination, corresponding to the radial gaps in an actual stator, are at $x = \pm 2v$ for a half-lapped core, and at $x = \pm 3v$ for a third-lapped core.

It is assumed that the radial gaps, although perfectly non-conducting, are infinitesimally thin. This simplifies the algebra, without introducing any significant error into the solution, since the mean magnetising force in the plane of the laminations does not appear in the idealised model. For the more general work described in the companion paper, a better representation of the gaps is necessary.

3. NOTATION AND DERIVATION OF THE EQUATIONS

The work on the idealised model of a core preceded the more general work described in the companion paper and gave the necessary ideas for the generalisation. However, it would be wasteful to repeat the derivation of the equations, which will be taken as required from the companion paper. They were obtained by integrating Maxwell's equations across the lamination and by introducing the assumption that the mean values of the magnetising force and flux density across the lamination were equal to the averages of their values on the two faces. In this way, the electromagnetic fields in each lamination can be described by five scalar quantities, each a function only of x, y and time, t.

S and s are scalar potentials which define the symmetric and antisymmetric parts, respectively, of the x and y components of the magnetising force. Thus, on one face of the lamination the surface magnetising force is the gradient of $S-s$, and on the other face it is the gradient of $S+s$.

B and b are the symmetric and antisymmetric parts, respectively, of the axial flux density.

T is a stream function which defines the mean value of eddy current density in the plane of the lamination.

The other notation required is straightforward.

a is the half-thickness of the lamination.

h is the thickness of non-magnetic material between laminations.

μ_0 is the fundamental constant of permeability.

μ_r is the relative permeability of the core-plate material, assumed to be constant and isotropic.

∇^2 is the two-dimensional Laplacian operator.

ρ is the resistivity of the core-plate material.

ω is the circular frequency.

With this notation, and using the representation of alternating fields by complex algebra, equations 10, 16 and 12 of the companion paper become:

$$T = \frac{s}{a} + \frac{B}{\mu_0\mu_r} + constant, \qquad \ldots\ldots (1)$$

$$\nabla^2 S = \frac{2b}{\mu_0(2a\mu_r+h)}, \qquad \ldots\ldots (2)$$

$$\nabla^2 T = \frac{j\omega}{\rho} B. \qquad \ldots\ldots (3)$$

From the symmetry of the problem, T, S, s, B and b must all be even functions of y. The remaining equations will be treated separately for the two types of lapping.

S is undefined to the extent of a solution of Laplace's equation. Since this plays no part in determining the eddy currents, it will be ignored and set to zero.

4. THE SOLUTION FOR HALF-LAPPED CORES

It is obvious from the symmetry of the half-lapped core that $S = 0$ and $b = 0$ and that T, s, and B are all even functions of x. Continuity of the scalar potential between laminations (Equation 14 of the companion paper) therefore gives

$$B = \frac{\mu_0}{h}\left[s(x,y) + s(x-2v,y)\right] \text{ for } x>0.$$

Because of the symmetry, there is no need to consider $x<0$, and the symmetry also permits the last equation to be rewritten as

$$B = \frac{\mu_0}{h}\left[s(x,y) + s(2v-x,y)\right] \text{ for } x>0. \qquad \ldots\ldots (4)$$

To obtain useful equations, it is necessary to divide s and T into symmetric and antisymmetric parts with respect to $x=v$ in the half-lamination for which $0<x<2v$:

$$s_1(x,y) = \tfrac{1}{2}\left[s(x,y) - s(2v-x,y)\right],$$
$$s_2(x,y) = \tfrac{1}{2}\left[s(x,y) + s(2v-x,y)\right],$$
$$T_1(x,y) = \tfrac{1}{2}\left[T(x,y) - T(2v-x,y)\right],$$
$$T_2(x,y) = \tfrac{1}{2}\left[T(x,y) + T(2v-x,y)\right],$$

giving $s = s_1 + s_2$ and $T = T_1 + T_2$. Equation 4 shows that B is necessarily symmetric with respect to $x=v$. Substituting these forms in equations 1, 3 and 4 gives, after some rearrangement and after absorbing the arbitrary constant of equation 1 into T_2,

$$B = 2\frac{\mu_0 s_2}{h}, \qquad \ldots\ldots (5)$$

$$T_2 = \left(\frac{1}{a} + \frac{2}{h\mu_r}\right)s_2, \qquad \ldots\ldots (6)$$

$$T_1 = \frac{s_1}{a}, \qquad \ldots\ldots (7)$$

$$\nabla^2 s_2 = \frac{2j}{d^2}s_2, \qquad \ldots\ldots (8)$$

$$\nabla^2 s_1 = 0, \qquad \ldots\ldots (9)$$

$$\text{in which } d^2 = \frac{(2a+\mu_r h)\rho}{a\mu_r\mu_0\omega} \qquad \ldots\ldots (10)$$

and so d is the skin-depth of a composite material of resistivity $\frac{(2a+h)\rho}{2a}$ and permeability $\frac{\mu_0\mu_r(2a+h)}{2a+h\mu_r}$. These are exactly the

resistivity and permeability used in a homogeneous[1] representation of a laminated core. Although the distribution of axial flux is changed by the gaps between laminations, the partial differential equation satisfied by the axial flux density remains the same as if there were no gaps. Since $\frac{2a}{\mu_r}$ will usually be much less than h, the permeability of the iron is of little importance in the equations; that is the justification for assuming it to be constant.

The boundary conditions are that T is constant around the edge of the lamination, which implies that $T_1 = 0$ at $y = \pm w$, T_2 = constant at $y = \pm w$, and $T_1 + T_2$ = the same constant at $x = \pm 2v$. This implies, through equations 5, 6 and 7, that $s_1 = 0$ at $y = \pm w$ and that B and s_2 are constant at $y = \pm w$. It is striking that the axial flux density at the surface of the stack of laminations is uniform whether or not there are gaps in the core.

Solutions of equations 8 and 9 which satisfy the boundary conditions at $y = \pm w$ must take the forms

$$s_1 = \sum_{n=1}^{\infty} a_n \cos\left(\frac{(2n-1)\pi y}{2w}\right) \frac{\sinh\left(\frac{(2n-1)\pi(x-v)}{2w}\right)}{\sinh\left(\frac{(2n-1)\pi v}{2w}\right)}, \qquad \ldots\ (11)$$

$$s_2 = \frac{hB_0}{2\mu_0} \frac{\cosh\left(\frac{(1+j)y}{d}\right)}{\cosh\left(\frac{(1+j)w}{d}\right)} + \sum_{n=1}^{\infty} b_n \cos\left(\frac{(2n-1)\pi y}{2w}\right) \frac{\cosh\left(\beta_n(x-v)\right)}{\cosh(\beta_n v)}, \qquad \ldots\ (12)$$

where $\beta_n^2 = \frac{2j}{d^2} + \frac{(2n-1)^2\pi^2}{4w^2}$,

and B_0 is the axial flux density at the surfaces of the stack of laminations, $y = \pm w$. The coefficients a_n and b_n can be determined by Fourier analysis of the remaining boundary conditions. Symmetry ensures continuity of T at $x = 0$ and also implies that $\partial T/\partial x = 0$ at $x = 0$, giving

$$\frac{\partial}{\partial x}\left[s_1 + \left(1 + \frac{2a}{h\mu_r}\right)s_2\right] = 0 \text{ at } x = 0.$$

The condition that T must have the same constant value at $x = 2v$ as at $y = w$ gives

$$s_1 + \left(1 + \frac{2a}{h\mu_r}\right)s_2 = \left(1 + \frac{2a}{h\mu_r}\right)\frac{hB_0}{2\mu_0} \text{ at } x = 2v.$$

These equations, together with equations 5 to 7, give a complete solution for the electromagnetic fields in this idealised representation of a half-lapped core.

5. THE SOLUTION FOR THIRD-LAPPED CORES

Finding the solution for an idealised third-lapped core was more complicated than might have been expected after the simplicity of the solution for half-lapped cores. It will not be possible to present the equations in the space available, but the way in which they were obtained will be described.

The biggest difference between the two solutions is that it is not possible to develop a set of equations for third-lapped cores on the assumption that the mean scalar potential, S, is zero. It is necessary to divide each of T, S, s, B and b into symmetric and antisymmetric parts in each of the three intervals $-3v \leq x \leq -v$, $-v \leq x \leq v$, and $v \leq x \leq 3v$. By use of symmetry, these six functions can be reduced to three for each of T, S, s, B and b. Both equation 13 and equation 14 of the companion paper are required, as well as equations 1 to 3 of the present paper, and finally it is possible to reduce the fifteen sets of equations to two sets of three simultaneous partial differential equations.

When this was done, it became possible to see that the mean scalar potential, S, had little effect on the axial flux density and the eddy currents. Since the mathemetical model was already highly simplified, there would have been no gain in accuracy in calculating this small effect; moreover, there is little value in bringing S into a linear calculation, since the radial and circumferential components of the magnetising force are more strongly affected by the non-linearity of the magnetisation curve than any other components of the electromagnetic fields. For these reasons, the equations were simplified by assuming that the same pattern of axial flux density existed in all three parts of the lamination, which is equivalent to supposing that the axial flux density is not influenced by S.

After this simplification has been made, it can be shown that the axial flux density, B, is constant along the surfaces of the stack of laminations and that B satisfies the same complex diffusion equation as in half-lapped cores (equation 8, with s_2 replaced by B). Thus B has the same form as before (equation 12 multiplied by $\frac{2\mu_0}{h}$) but the coefficients b_n are different. The rest of the solution, including these coefficients, can be determined by solving equation 3. The stream function, T, can be expressed as the sum of a single solution of the complex diffusion equation, proportional to B, and a solution of Laplace's equation different in each of the three parts of the lamination. The mean scalar potential, S, obtained from this solution is not zero, but its effect on T and B is small.

6. PATTERN OF AXIAL FLUX DENSITY

All the results which follow are expressed per unit and are based on the same axial flux density at the surface of the stack of laminations. The reason is that, in an actual stator, most of the axial flux is carried in and around the teeth. This dominates any differences that different designs may produce in the back of core and so a unit axial flux density at the surface is the most reasonable basis for comparison.

The pattern of axial flux density is shown in Fig. 3. For half-lapped cores there is a low ridge along the radial gaps, whose height is about 10% of the axial flux density at the surface. There is a similar low ridge in third-lapped cores, but it is only about two thirds as high as in a half-lapped core. Such a pattern has been observed experimentally at the Central Research Laboratories of the Central Electricity Generating Board[3], but the fields were not homopolar and quantitative comparison was impossible.

7. EDDY CURRENT STREAM LINES

Eddy current stream lines have been plotted for half-lapped (Fig. 4) and third-lapped (Fig. 5) cores. The total current between two stream lines is roughly the same in all the figures. Some of the figures seem surprising, but it has been checked that they are the solutions of equation 3 for the patterns of axial flux shown in Fig. 3.

8. EFFECT OF CIRCUMFERENTIAL WIDTH OF LAMINATIONS

One application of the work has been to study the effect of varying the width of laminations. A size of core typical of a 660 MW, 50 Hz, two-pole turbogenerator was taken and calculations were made for various numbers of laminations in the same layer, the circumferential width of each lamination being inversely proportional to this number.

The total voltage induced by axial flux in a pole-pitch (Fig. 6) and the total eddy current loss (Fig. 7) were calculated by adding sinusoidally distributed idealised solutions and should be treated cautiously for the wider laminations. For a typical width of lamination for an actual generator, the total voltage (proportional to the total axial flux) is about 20% greater than it would have been in a core made of continuous laminar rings and there is a small difference of phase. The total eddy current loss is about a third greater than it would have been in a core made of continuous laminar rings. A theoretical model developed at Imperial College also predicts effects of this order[4].

Both the total voltage and the total eddy current loss decrease as the circumferential width of the laminations increases.

9. EXPERIMENTAL EVIDENCE

There is no direct experimental confirmation of the predicted effects, but, as well as the qualitative behaviour measured by the CEGB (discussed in Section 6), there is some quantitative evidence, admittedly circumstantial. The work has been used to correct NEI Parsons' existing three-dimensional calculation of electromagnetic fields near the end of a generator stator, which is based on a homogeneous model. With the correction, the prediction of total losses attributable to axial flux is within 10% of the total deduced from local measurements of loss densities[5]. Predictions of temperature rises have also been improved by including the additional loss caused by axial flux at the radial gaps[6]. Thus there is some reason to suppose that the idealised model is a fair approximation to the effect of the radial gaps sufficiently far, say 100 mm, from the core end.

10. CONCLUSIONS

The effect of gaps between laminations on axial flux and eddy currents has been calculated for an idealised core. There is a low ridge of axial flux density at the gaps, which may increase the total axial flux by a fifth, and the total eddy current loss by a third.

11. ACKNOWLEDGEMENTS

The work formed part of a joint programme of research by NEI Parsons Limited and the Central Electricity Generating Board.

The authors wish to thank NEI Parsons for permission to publish and Dr. D.A.H. Jacobs of the CEGB for his encouragement.

12. REFERENCES

1. Jacobs, D.A.H. The calculation of magnetic fluxes and eddy currents in generator stator cores. Proc. 1st COMPUMAG Conf., Oxford, April 1976, Section 7, p. 255.
2. Phemister, T.G. General discrete equations for laminated cores. Proc. 2nd COMPUMAG Conf., Grenoble, September 1978.
3. Jackson, R.L. Private communication.
4. Carpenter, C.J. Private communication.
5. Platt, R. Private communication.
6. Morris, S.D. Private communication.

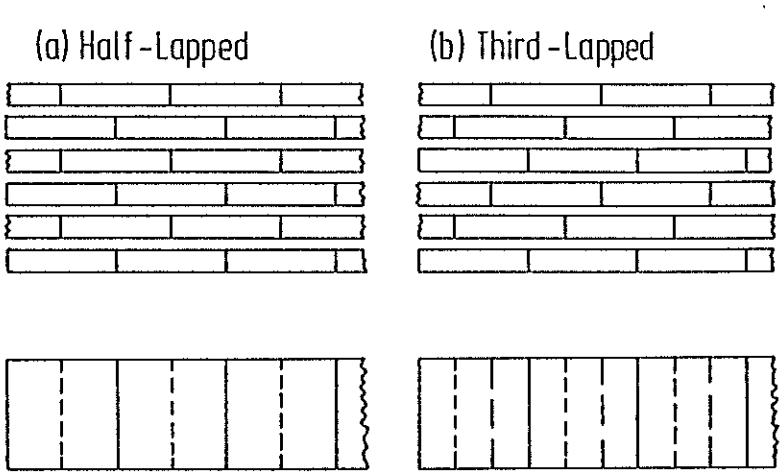

FIG.1 TYPES OF LAPPING

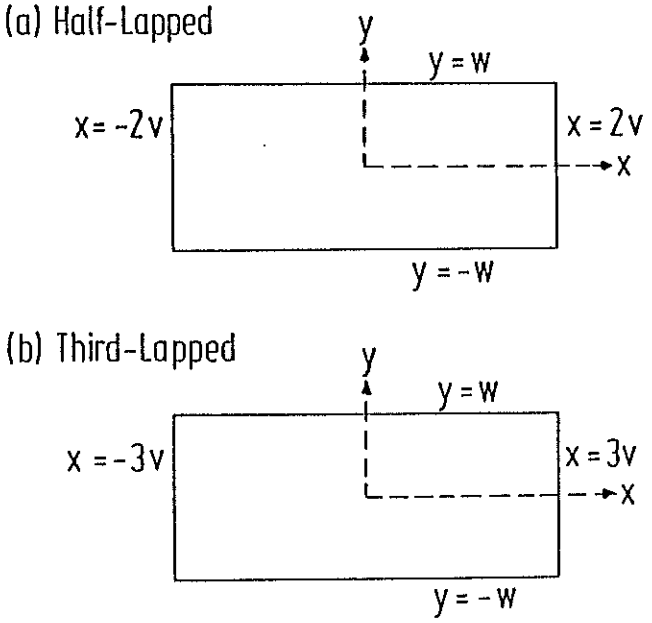

FIG.2 CO-ORDINATE SYSTEM

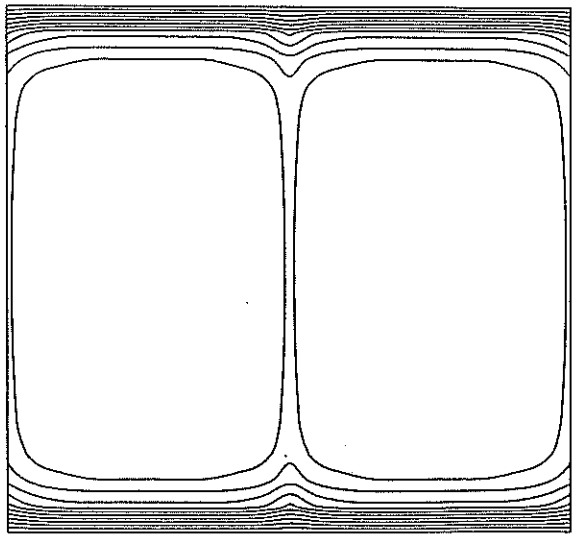

(a)

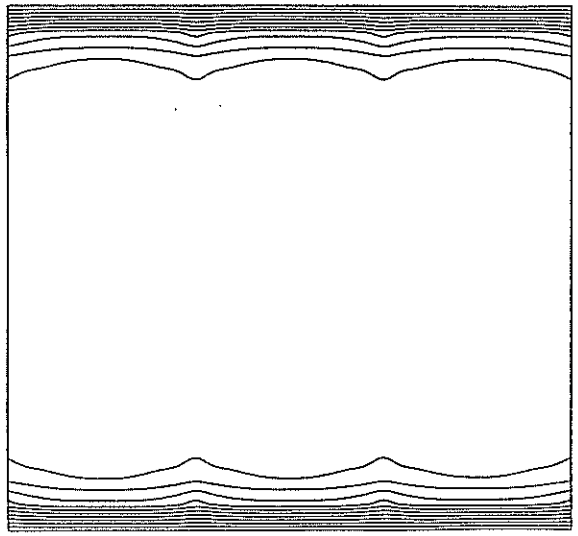

(b)

FIG 3 TYPICAL CONTOURS OF AXIAL FLUX DENSITY

(a) HALF LAPPED CORE

(b) THIRD LAPPED CORE

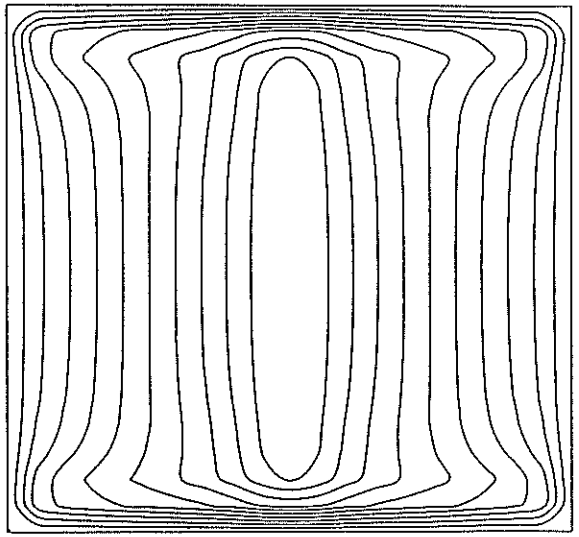

(a)

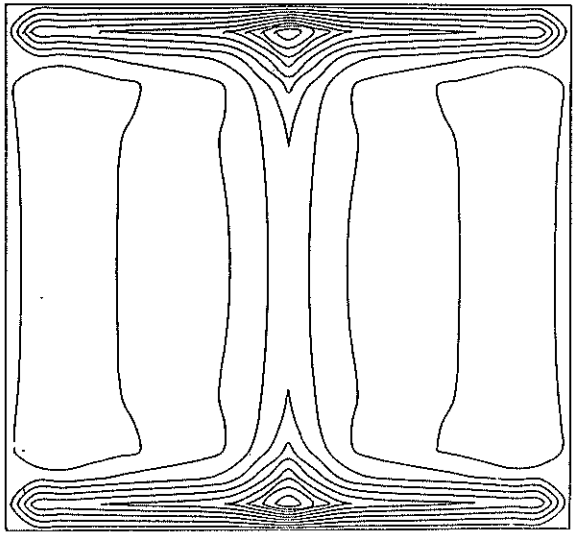

(b)

FIG 4 TYPICAL EDDY CURRENT STREAMLINES IN HALF LAPPED CORE

(a) IN PHASE WITH SURFACE FLUX DENSITY

(b) IN QUADRATURE WITH SURFACE AXIAL FLUX DENSITY

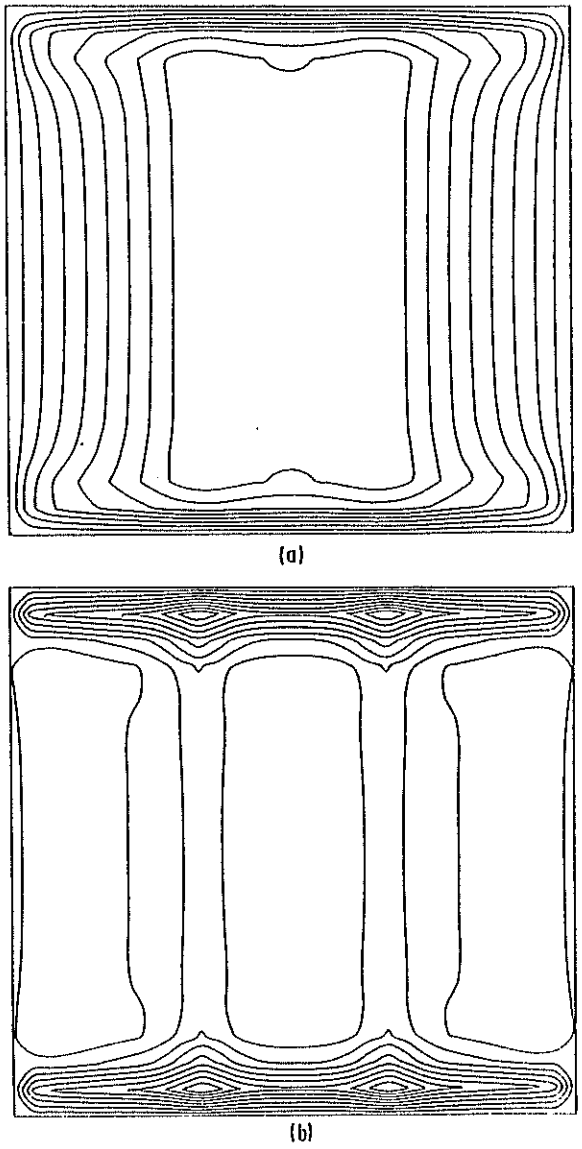

FIG 5 TYPICAL EDDY CURRENT STREAMLINES IN THIRD LAPPED CORE
(a) IN PHASE WITH SURFACE FLUX DENSITY
(b) IN QUADRATURE WITH SURFACE AXIAL FLUX DENSITY

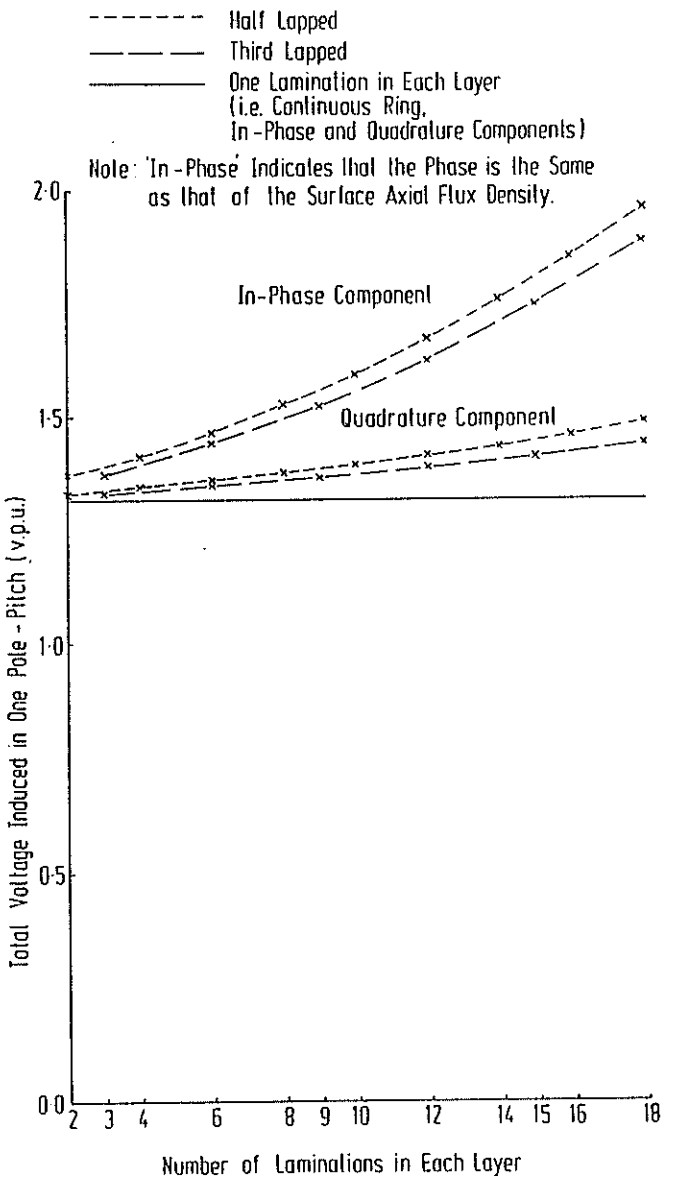

FIG 6 VARIATION OF TOTAL VOLTAGE INDUCED ROUND A POLE PITCH WITH NUMBER OF LAMINATIONS PER LAYER.

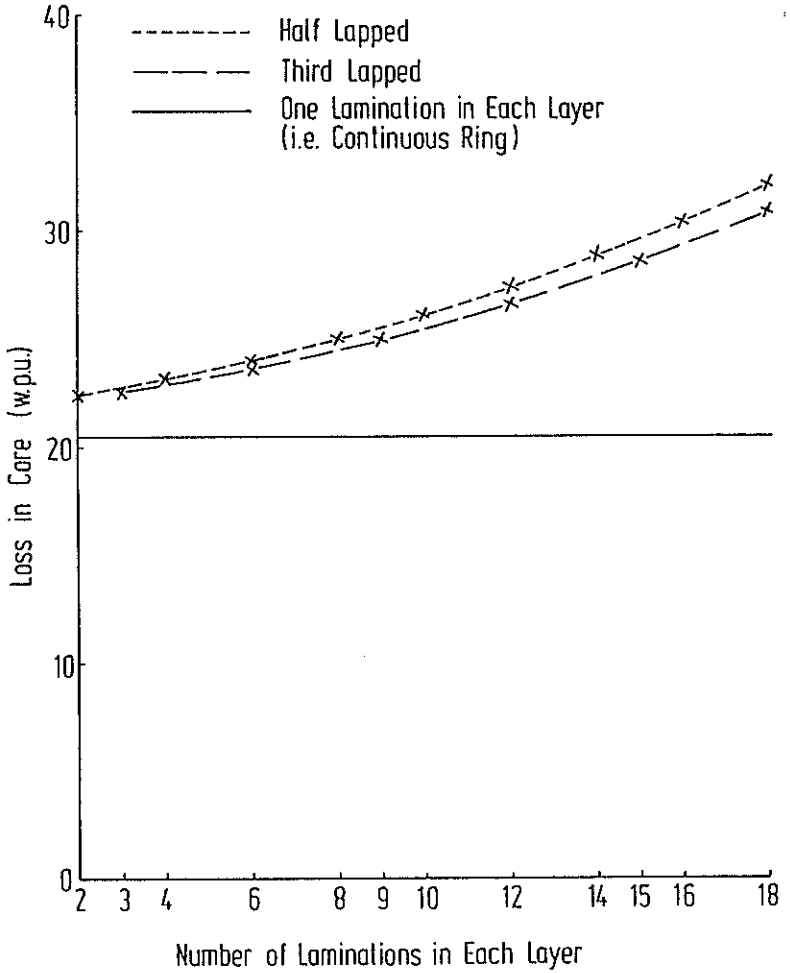

FIG.7 VARIATION OF TOTAL EDDY CURRENT LOSS IN CORE WITH NUMBER OF LAMINATIONS PER LAYER.